Citation
Tran, D.T. and Pham, T.M. and Hao, H. and Chen, W. 2021. Numerical study on bending response of precast segmental concrete beams externally prestressed with FRP tendons. Engineering Structures. 241: ARTN 112423. http://doi.org/10.1016/j.engstruct.2021.112423

Numerical Study on Bending Response of Precast Segmental Concrete Beams Externally Prestressed with FRP Tendons

Duong T. Tran[1], Thong M. Pham[2], Hong Hao[3], Wensu Chen[4]

ABSTRACT

This study numerically investigates the bending response of dry key-jointed precast segmental concrete girders/beams (PSCBs) prestressed with external fiber reinforced polymer (FRP) tendons by using commercial finite element analysis (FEA) software Abaqus/CAE. The experimentally-validated model was used to conduct an intensive parametric analysis with a focus on the second-order effect. There has not been a similar numerical study of PSCBs with external FRP tendons in the published literature yet. The results showed that due to the rectilinear rigid-body bending shape, the behavior of PSCBs with external tendons was similar to that with internal tendons only if placing the deviators next to the opening joints. The second-order effect on the beam's behavior and the harping effect on the tendon stress at deviators became more obvious when the deviators were located away from the opening joints. Both the second-order and harping effect were proportionate to the beam's displacement. Therefore, using a high reinforcing index (ω) or a low span-to-depth ratio (L/d_p) could mitigate the second-order and harping effect at the ultimate stage because the ultimate displacement of the beam decreased when increasing ω or reducing L/d_p. Commonly-used CFRP tendons (Young's modulus E_p = 145 GPa) were found to be the optimum to replace steel tendons in PSCBs with

[1] PhD Scholar, Centre for Infrastructural Monitoring and Protection, School of Civil and Mechanical Engineering, Curtin University, Kent St, Bentley, WA 6102, Australia. ORCID: https://orcid.org/0000-0001-7624-5977. Email: t.tran86@student.curtin.edu.au
[2] Senior Lecturer, PhD, Centre for Infrastructural Monitoring and Protection, School of Civil and Mechanical Engineering, Curtin University, Kent St, Bentley, WA 6102, Australia. Email: thong.pham@curtin.edu.au (Corresponding author)
[3] John Curtin Distinguished Professor, Centre for Infrastructural Monitoring and Protection, School of Civil and Mechanical Engineering, Curtin University, Kent St, Bentley, WA 6102, Australia. Email: hong.hao@curtin.edu.au (Corresponding author)
[4] Senior lecturer, PhD, Centre for Infrastructural Monitoring and Protection, School of Civil and Mechanical Engineering, Curtin University, Kent St, Bentley, WA 6102, Australia. Email: wensu.chen@curtin.edu.au

external tendons because they offered the PSCBs similar strength and ductility compared to steel tendons. The use of high-modulus CFRP tendons (e.g. E_p = 200 GPa) improved the stiffness and strength of PSCBs but greatly reduced the beam's ductility. Lastly, the analytical analyses showed that the existing models yielded unconservative estimations of the effective depth (d_{pu}) and stress (f_{pu}) of external FRP tendons at the ultimate stage in PSCBs.

Keywords: Precast segmental concrete structures (PSCBs); External tendons; Second-order effect; FRP; Unbonded tendons; Flexural behavior; Abaqus; Numerical simulation.

1. INTRODUCTION

Precast segmental concrete girders/beams (PSCBs) offer many benefits such as enhancement in the construction quality control and speed, and reduction in the construction cost and disruption to the environment as compared to the conventional cast-in-place monolithic structures [1-3]. The joint condition in PSCBs can be either dry or epoxied and the use of dry joints can further accelerate the construction process in comparison with the use of epoxied joints [4]. To join segments in PSCBs together, a post-tensioning technique with either internal or external tendons can be used. As reported in the previous studies [5-7], the use of external tendons can simplify and expedite the installation of the tendons and thus decrease the construction cost compared to internal tendons. Also, as external tendons are placed outside the structure, their use reduces the maintenance cost and the dead load of the structure due to a reduction in the structure's web thickness. External post-tensioning is also deemed as one of the most effective techniques to strengthen or rehabilitate existing structures [8]. Therefore, PSCBs prestressed with external steel tendons have been widely researched lately [3, 9-11]. However, since segments in PSCBs are mainly connected to each other via steel tendons, the corrosion problems synonymous with steel material can cause catastrophic damage or even collapse of the structures [11-14]. To deal with the corrosion problems, replacing steel tendons with nonmetallic corrosion-free tendons such as fiber-reinforced polymer (FRP) tendons can be a promising solution. From the foregoing discussion, the concept of using external FRP tendons in PSCBs with dry joints can be considered as cost-effective and sustainable. Nonetheless, even though the use of FRP tendons in monolithic structures has been intensively studied, only limited studies have been reported recently of using FRP tendons to replace steel tendons in internally prestressed PSCBs [14-16]. There is so far only one study that investigates the application of external FRP tendons in PSCBs [11]. More studies are, hence, deemed necessary to substantiate the feasibility of using external FRP tendons in segmental structures.

Furthermore, it is well known that the major reason for the differences in the response between structures internally and externally prestressed with tendons is the second-order effect which is inherent in a structure having an external prestressing system. As a beam prestressed with external tendons is moving downwardly due to the applied loads, the eccentricity of the tendons between the anchorages or deviators with respect to the neutral axis of the section reduces because of its lack of restraint to the beam [17-19]. This phenomenon is known as the second-order effect which is not observed in a beam with internal tendons as the tendons are restrained along the tendons' entire length and thus the effective depth of the internal tendons does not change with the beam's deformation. However, unlike monolithic beams on which the second-order effect has been well documented, there is no study that comprehensively investigates the second-order effect on segmental beams, to the best of the author's knowledge. As pointed out in the study by Tran et al. [16], the bending shape of a segmental beam is very different from that of the corresponding monolithic beam, i.e. a rectilinear rigid-body bending shape for the former while a curvilinear bending shape for the latter. The second-order effect in a PSCB is logically different from that in a monolithic beam.

Therefore, to estimate the bending resistance of a PSCB prestressed with external FRP tendons, the accurate predictions of the effective depth (d_{pu}) and stress of the tendons (f_{pu}) at the ultimate stage are imperative. The tendon's ultimate effective depth (d_{pu}) is the depth of the external tendon at the ultimate load of the beam. Unlike bonded tendons where a simple sectional analysis can be utilized to estimate the tendons stress, the analysis of a structure with unbonded tendons is more complicated because the unbonded tendons are only anchored to the beam through the end anchorages [20-23] and thus an entire member-based analysis is required to estimate the tendon stress [16, 24]. For a structure using external tendons, the analysis is even far more complex. The complexity results from the second-order effect which decreases the eccentricity of the external tendons compared to internal tendons whose eccentricity remains unchanged under loading. There have been no available models to predict d_{pu} and f_{pu} of external FRP tendons in PSCBs reported in the literature yet. One of the common methods to predict d_{pu} and f_{pu} of external tendons in PSCBs is to use the models intended for monolithic beams prestressed with external tendons. However, the accuracy of those models in the case of PSCBs requires careful verification.

Based on the aforementioned research gaps, this study numerically investigates the bending response of dry key-jointed PSCBs post-tensioned with external FRP tendons by using commercial FEA software Abaqus/CAE [25]. This study successfully develops a 3D FE model of PSCBs with external FRP tendons which is validated against the test results from other studies. There has not been a similar numerical analysis of PSCBs post-tensioned with external FRP tendons reported in the open literature yet. An intensive parametric investigation on the effect of various parameters on the bending response of the PSCBs is conducted based on the experimentally validated model. Finally, the accuracy of existing models to predict d_{pu} and f_{pu} of external FRP tendons in PSCBs is evaluated.

2. FINITE ELEMENT MODEL DEVELOPMENT

2.1. *General*

A PSCB post-tensioned with external FRP tendons under quasi-static loads was simulated by using Abaqus/CAE [25]. The results of the numerical models were carefully validated with the test results from the previous studies. Four PSCBs tested in the previous studies were adopted for model verification, including two dry key-jointed four-segment PSCBs post-tensioned with external CFRP tendons (beam C-D) and external steel tendons (beam S-D) in the study by Le et al. [11], a dry key-jointed seven-segment PSCB post-tensioned with external steel tendons (beam D2) in the study by Aparicio et al. [9], and a dry key-jointed four-segment PSCB post-tensioned with internal unbonded CFRP tendons (beam C3) in the study by Le et al. [14]. It is noteworthy that there is only one study of dry-jointed segmental beam externally prestressed with FRP tendons reported in the open literature, i.e. beam C-D, to the best of the authors' knowledge. Thus, the numerical model could only be validated against this beam. To further demonstrate the reliability of the numerical model, and also for comparison, the model is further validated against other types of beams that are similar to the objectives of this study, namely dry-jointed segmental beams prestressed with external steel tendons or internal unbonded FRP tendons. Those types of beams also serve as the benchmarks to compare the performance between FRP and steel tendons and investigate the second-order effect in segmental beams, respectively. The PSCBs post-tensioned with external steel tendons (beams S-D and D2) and the PSCB post-tensioned with internal unbonded CFRP tendons (beam C3) were chosen due to the availability of the beam design, material properties, test setup, and the beam's behavior reported in the previous studies [9, 11, 14].

Beams C-D and S-D were simply supported and had a T-section with a total height of 400 mm, flange width of 600 mm, and span of 3600 mm (**Fig. 1**). Beam C3 had the same test setup and beam design as beam C-D's except that the tendons were placed inside metal ducts of 40 mm in diameter which were embedded inside the beam. For the simply-supported beam D2, it had a box section with a height of 600 mm, flange width of 1200 mm, and span of 7200 mm. More details about beams C-D and S-D are presented in the study by Le et al. [11] while further details about beams C3 and D2 can be found in the studies by Le et al. [14] and Aparicio et al. [9], respectively.

Due to the symmetry of the beams' section and to reduce the computational effort, only half of the beams' section was modeled in Abaqus/CAE [25]. The beams were statically loaded using a displacement-controlled method as in the laboratory tests. Solid hexahedral elements C3D8R (reduced integration with hourglass control and 8-node linear brick) were used to model the concrete elements, steel plates, anchor system, and tendons, whereas 2-node linear 3-D truss elements T3D2 were used to model the auxiliary longitudinal and transverse reinforcements.

The Predefined Fields tool in Abaqus/CAE [25] was utilized to apply prestresses to the tendons. Initial stresses for an element or a set of elements can be defined directly by inputting the stress value in Predefined Fields. It is worth noting that a separate step should be created for Abaqus to only apply the initial stresses in order to achieve the equilibrium state.

Based on the mesh size convergence study (80 mm, 40 mm, 20 mm, and 10 mm), the concrete beam was meshed with the mesh size of 40 mm except for the region within 200 mm on both sides of the joints where 20-mm mesh size was chosen to better capture the response of the critical region (**Fig. 2**). For other components, a 20-mm mesh size was used for tendons and auxiliary reinforcements while the mesh size of 40 mm was adopted for the anchor system and steel plates.

2.2. *Constitutive material law*

2.2.1. Concrete

With the ability to simulate the elastic and inelastic response of concrete under compression and tension, the concrete damage plasticity (CDP) model in Abaqus/CAE [25] was adopted to simulate the concrete material in this study. The CDP model's parameters are summarized in **Table 1** while the stress-strain curve for plain concrete under uniaxial compression proposed by Carreira and Chu [26] was adopted in this study. This stress-strain curve is expressed mathematically as follows:

$$\sigma_c = f_c^{'} \times \frac{\left(\varepsilon_c / \varepsilon_c^{'}\right) \times \beta}{\left(\varepsilon_c / \varepsilon_c^{'}\right)^{\beta} + \beta - 1} \quad (1)$$

$$\varepsilon_c^{'} = \left(168 + 0.71 f_c^{'}\right) \times 10^{-5} \quad (2)$$

where σ_c (MPa) and ε_c are the concrete compressive stress and strain; f'_c (MPa) and ε'_c are the concrete compressive strength and the corresponding strain at f'_c, respectively; and β is a material factor which depends upon the stress and strain relationship and can be determined by **Eq. (3)** where E_c (MPa) is the concrete's elastic modulus.

$$\left(\frac{0.4f_c^{'}}{E_c\varepsilon_c^{'}}\right)^{\beta}-\beta\times\left(\frac{f_c^{'}}{E_c\varepsilon_c^{'}}-1\right)-1=0 \tag{3}$$

Regarding the constitutive model for concrete in tension, the bilinear stress-strain relationship suggested by Shahrooz et al. [27] was used. This stress-strain curve of concrete under uniaxial tension encompasses two linear lines: the first line ascends from the zero point (0, 0) to (ε_{cr}, f_{ct}) with f_{ct} and ε_{cr} being respectively the tensile strength and strain at cracking of concrete (concrete strain at f_{ct}), while the second line descends from (ε_{cr}, f_{ct}) to a strain of 10 times higher than the strain at f_{ct} with zero tensile stress ($10\times\varepsilon_{cr}$, 0).

$$\tilde{\varepsilon}_c^{in}=\varepsilon_c-\varepsilon_{0c}^{el}=\varepsilon_c-\frac{\sigma_c}{E_c} \tag{4}$$

$$\tilde{\varepsilon}_t^{ck}=\varepsilon_t-\varepsilon_{0t}^{el}=\varepsilon_t-\frac{\sigma_t}{E_c} \tag{5}$$

$$d_c=1-\frac{\sigma_c/E_c}{\sigma_c/E_c+\left(1/b_c-1\right)b_c\tilde{\varepsilon}_c^{in}}\ \text{with}\ b_c=0.7 \tag{6}$$

$$d_t=1-\frac{\sigma_t}{f_{ct}}\ \text{when}\ \varepsilon_t\geq\varepsilon_{cr} \tag{7}$$

The stress-strain relation of concrete is divided into two stages: elastic and plastic. The elastic stage under compression is assumed until the compressive stress exceeds 40% of f'_c while the elastic stage under tension ends when the tensile stress reaches f_{ct} (**Fig. 3**). In CDP model, the plastic response of concrete is modeled via stress-plastic strain ($\tilde{\varepsilon}_c^{pl}$ for compression and $\tilde{\varepsilon}_t^{pl}$ for tension) relationships taking into account the elastic stiffness degradation. In the plastic stage, due to the formation of micro-cracks in concrete, the elastic stiffness of concrete under unloading is damaged (**Fig. 3**). The elastic stiffness degradation is characterized by two damage variables in the CDP model (d_c for compression and d_t for tension). The values of the damage variables range from 0 to 1.0 in which 1.0 means the complete loss of strength of the material.

Users first need to input the stress versus inelastic strain data ($\tilde{\varepsilon}_c^{in}$ for compression and $\tilde{\varepsilon}_t^{ck}$ for tension which is also called as cracking strain) and the damage variables into Abaqus/CAE [25]. Inelastic compressive strains ($\tilde{\varepsilon}_c^{in}$), the cracking strain ($\tilde{\varepsilon}_t^{ck}$), and damage variables are determined by **Eqs. (4)-(5)**, in which σ_c and ε_c are the concrete compressive stress (MPa) and strain, respectively; σ_t and ε_t are in turn the concrete tensile stress and tensile strain; ε_{0c}^{el} and ε_{0t}^{el} are the elastic compressive and tensile strain of concrete, respectively. **Eq. (6)** was adopted from the study by Birtel and Mark [28] to determine d_c while **Eq. (7)** to calculate d_t is derived from the assumption of linear softening behavior of the concrete after cracking. Finally, Abaqus/CAE [25] automatically converts the inelastic strains into the plastic strains as per **Eqs. (8)** and **(9)**.

$$\tilde{\varepsilon}_c^{pl} = \tilde{\varepsilon}_c^{in} - \frac{\sigma_c}{E_c} \times \frac{d_c}{(1-d_c)} \tag{8}$$

$$\tilde{\varepsilon}_t^{pl} = \tilde{\varepsilon}_t^{ck} - \frac{\sigma_t}{E_c} \times \frac{d_t}{(1-d_t)} \tag{9}$$

Since no cracks in concrete were observed in the experimental tests [11, 14] and the numerical simulation in this study, it can be concluded that the tensile nonlinearity of concrete can be ignored for the beams with the configurations under the loading scheme used in this study. However, for different loading schemes as well as different beam configurations, cracks in concrete may appear as reported in the previous studies [29-32]. Therefore, the tensile nonlinearity of concrete is considered in the numerical model although the simulation results indicate no concrete tensile cracking damage.

2.2.2. Tendons and auxiliary reinforcements

An isotropic material model was used to model the steel low-relaxation strands whose stress (σ_p) and strain (ε_p) relationship was adopted from the study by Devalapura and Tadros [33] as shown in **Eq. (10)** where f_{pu} is the ultimate tensile strength of tendons. An orthotropic elastic material model was used for FRP tendons which exhibit a linear behavior until failure in the stress and strain relationship and behave primarily in the direction of the fibers. Finally, regarding the auxiliary steel reinforcements (longitudinal and transverse), they were simulated by an isotropic elastoplastic material model. More details as to the mechanical properties of the FRP tendons, steel tendons, and auxiliary steel reinforcements are tabulated in **Table 1** and **Fig. 3**.

$$\sigma_p \text{ (MPa)} = 6.895 \times \left[887 + \frac{27613}{\left\{ \left(112.4\varepsilon_p\right)^{7.36} + 1 \right\}^{1/7.36}} \right] \times \varepsilon_p \le f_{pu} \qquad (10)$$

2.3. *Boundary conditions and interactions*

Simply-supported beams were modeled with pinned and roller supports in Abaqus/CAE [25]. The surface-to-surface contact method was adopted to simulate the interactions between deviators/ducts and external/internal unbonded tendons (unbonded-tendon contact), and between the interfaces of the segments in PSCBs (joint contact). In the tangential direction, the Coulomb friction model was used with a friction coefficient of 0.7 [2, 4] for the joint contact and a friction coefficient of 0.24 [34] for the unbonded-tendon contact. In the normal direction, the “hard” contact type was adopted for both joint contact and unbonded-tendon contact. It is noteworthy that when the “hard” contact is given, a hard pressure-penetration relationship is rigorously enforced by Abaqus/CAE [25]. This means that the slave elements are not allowed to penetrate the master elements when they are in contact. Besides, tensile stresses are not transferable between two contacting surfaces when the “hard” contact is chosen.

Moreover, based on the assumed perfect bond between the concrete and the auxiliary steel reinforcements, these reinforcements were associated with the concrete beam by using the embedded region constraint. This constraint method was also used to connect the tendons to the anchor blocks. The embedded region constraint is used to embed an element or a set of elements in a host element in Abaqus. This technique is designed to model rebar reinforcement (embedded element) in concrete (host element) with an assumption of the perfect bond between the rebar and concrete. When the embedded region constraint is given, Abaqus automatically finds the geometric relations between the nodes of the embedded elements and that of the host elements. If a node of the embedded elements lies within the host elements, Abaqus eliminates the translational degrees of freedom of the node and the node becomes an embedded node. Then, the translational degrees of freedom of the embedded node are constrained to the degrees of freedom of the corresponding nodes of the host element based on the geometric location of the embedded node in the host element.

2.4. ***Validation of the numerical model***

The 3D FE models developed in the study were validated thoroughly against the test results from the previous studies [9, 11, 14] in terms of the applied load vs displacement curve, total joint opening, failure patterns, and ultimate stress of tendons. It is evident from **Figs. 4a** and **c** that the numerical model in this study was able to capture the flexural response of the dry key-jointed T-section PSCBs externally prestressed with CFRP (beam C-D) and steel tendons (beam S-D), and the PSCB internally prestressed with CFRP tendons (beam C3). For the box PSCB externally prestressed with steel tendons (beam D2), only the force-displacement curve of the second (or last) cycle was provided in reference [9] which was loaded up to 90% of its load-bearing capacity in the first cycle. The pre-loaded conditions in the first cycle could have caused damage to concrete and thus reduced the stiffness and the yielding force of the beam as observed in the previous studies [11, 14, 23]. Therefore, the initial stiffness of the numerical model was slightly higher than that of beam D2 at the second cycle, but the numerical model was able to simulate well the general response of the beam and particularly at the ultimate stage (**Fig. 4b**). The variations in the load-carrying capacity and ultimate displacement between the simulation and test results were respectively about 2% and 3% on average (**Table 2**). In terms of the total joint opening, the differences between the simulation and test results ranged from 5-7% (**Table 2**). The numerical model was also capable of predicting the similar failure mode of the beams compared to the experimental results (**Fig. 4**). For example, at failure of beam S-D and beam C-D, concrete was crushed at the middle joint (joint 2) while the other joints (Joint 1 and 3) were spared [11]. This failure mode was captured by the FE model as illustrated in **Figs. 4c** and **4d**. For the sake of brevity, only the failure pattern of beams S-D and C-D is shown. It should be noted that concrete is deemed to fail in compression when the compressive damage variable d_c approaches 1.0 in this study.

Regarding the ultimate stress of the tendons at the midspan, the results from the numerical models were also compared with the experimental results in **Table 2**. As observed in the study by Tran et al. [16], there was a variation in the stress of tendon across its cross-section because of the bending effect, whereby the highest stress was recorded at the outermost fiber of the tendons while the lowest stress was recorded at the innermost fiber (see **Fig. 5** for the location of the outermost, central and innermost fibers of the tendons). Except for beam D2 whose tendon's strain data can be considered at the central fiber because it was averaged from three strain gauges bonded on three out of six external wires of the tendons, the location (outermost, central, or innermost fibers) where the strain was measured in beams C-D, S-D, and C3 was not provided in the previous studies [11, 14]. Hence, the ultimate tendon stresses at three different critical fibers including the outermost, innermost, and central fibers in the numerical models ($f_{pu,out}$, $f_{pu,in}$, and $f_{pu,cen}$ respectively) were compared to the test results in those beams (C-D, S-D, and C3). As summarized in **Table 2** that there was good agreement between the numerical models and experiments in terms of the ultimate tendon stress in the PSCBs using external tendons (C-D, S-D, and D2). The discrepancies between the simulations and experiments were less than 5% (**Table 2**). Nevertheless, the difference between the simulated ultimate tendon stress at the outermost and innermost fibers vs the test results in beam C3 (a

PSCB with internal tendons) was +31% and -15%, respectively (**Table 2**). This huge difference in the tendon stress between the outermost and innermost fiber could be attributed to the concentration of bending deformation at the middle joint of the PSCB [16]. It should be noted that the ultimate tendon stress at the central fiber in beam C3 was just 7.8% greater than the test results (**Table 2**). Tran et al. [16] found that unlike a monolithic beam where the bending deformation or curvature was more uniformly distributed within the flexural span and therefore the variation in the tendon stress between the outermost and innermost fibers was insignificant, the curvature was highly localized at the middle joint location in a segmental beam prestressed with internal tendons (a rigid body mechanism), which resulted in the substantial difference in the stress distribution across the tendon's cross-section. It is worth noting that the large discrepancy in tendon stress between the outermost and innermost fiber at the midspan was not seen in the PSCBs prestressed with external tendons (beams C-D, S-D, and D2) (**Table 2**), although the rigid body mechanism was also observed in those beams. This is because the external tendons were placed outside in those beams and thus the tendons were not affected by the concentration of the beam's bending deformation at the middle joint. However, the harping/bending effect at the deviators in the PSCBs with external tendons caused a significant variation in the tendon stress across the tendon's cross-section at the deviators (**Table 2**). When the tendons are bent around a deviator, the bending causes additional stress at the fiber away from the centroid of the tendon's cross-section [35]. For example, the ultimate tendon stress at the outermost fiber was higher than that at the central fiber by 17% in beam C-D (**Table 2**). Similar results were also observed in the previous experimental studies [35, 36] which indicated that the harping/bending angle of 3-5° increases the FRP tendon's stress at the outermost fiber by 12-35% as compared with the stress at the central fiber.

The above comparison with the experimental results has demonstrated the accuracy of the 3-D FE model developed in this study in capturing the behavior of a PSCB post-tensioned with external or internal unbonded tendons. This validated model is utilized to carry out further investigations on the structural behavior of PSCBs in the next sections.

3. PARAMETRIC STUDY

From the existing knowledge gaps about the second-order effect on segmental concrete beams as discussed in section 1, this section is dedicated to providing more insights into this matter. It should be noted that the reduction in the external tendon's eccentricity (or effective depth) when the beam deflects is discussed via the reduction in the effective depth of the tendons in this study. To achieve that goal, a rigorous parametric analysis has been carried out, which covered primary parameters [8, 15, 16, 37] including the position of deviators with regard to the beam's supports (L_d), span-to-depth ratio (L/d_p), prestressing reinforcement ratio (ρ_p) and effective prestressing stress (f_{pe}) (see **Fig. 6**). The effect of concrete compressive strength and the number of segments on the bending response of PSCBs with internal unbonded tendons were found to be insignificant [15]. Since PSCBs with internal unbonded tendons serve as a reference case, it is believed that those parameters (concrete compressive strength and the number of segments) also have a negligible effect on PSCBs with external tendons; thus, those parameters were not covered in this parametric analysis. However, more studies are needed to confirm this assumption. The height of the beam was varied rather than the beam's span (**Fig. 6**) when investigating the span-to-depth ratio (L/d_p) to maintain the same number of segments and the position of loading points which can significantly affect the beam's response. In addition, enlightened by some previous studies [8, 38, 39] and to reduce the number of numerical models, the effect of ρ_p and f_{pe} can be represented by the reinforcing index ω ($= \rho_p \times f_{pe} / f'_c$). Another reason for the combination is because ρ_p and f_{pe} exhibit similar influences on the bending response of PSCBs post-tensioned with internal unbonded tendons which serve as a reference for PSCBs with external tendons. Increasing ρ_p or f_{pe} enhanced the loading resistance but reduced the ductility of the beams [15, 16]. Lastly, the effect of different types of tendon's material (CFRP, high-modulus CFRP, AFRP, BFRP, GFRP, and steel tendons) is also discussed in this section.

The beam's configurations and materials used in the parametric analysis were similar to those described in section 2 except that a straight tendon profile was used to simplify the modeling process. In parametric simulations the reinforcing index (ω), beam's height (h) and the position of deviators (L_d) were varied. The beam configurations used in this parametric analysis are depicted in **Fig. 6** while the mechanical properties of materials are tabulated in **Table 1**.

Based on the range of the parameters used in the previous experimental studies on PSCBs [3, 6, 9-11, 14, 40-45] and monolithic beams [36, 46-48] prestressed with steel or FRP tendons, the investigated L/d_p and ρ_p had the values from 11 to 20 and 0.1% to 0.25%, respectively. The investigated range of f_{pe} was 18-50% of the CFRP tendon's tensile strength ($f_{pu,CFRP}$). The lower and upper level of f_{pe} was chosen to be able to compare with GFRP and steel tendons, respectively. On the one hand, according to ACI 440.4R-04 [24], the effective prestressing stress of GFRP, as well as AFRP, tendons should not exceed 40% of their tensile strength due to their low creep-rupture characteristics, and 40% of the GFRP tendon's strength is equivalent to 18% of $f_{pu,CFRP}$. On the other hand, the initial prestressing level (not counting any losses of prestressing) of steel tendons is limited to 70% of its tensile strength following ACI 318-19 [49], and 50% of $f_{pu,CFRP}$ equals 66% of the steel tendon's tensile strength. As a result, the surveyed value of the reinforcing index ω (= $\rho_p \times f_{pe} / f'_c$) ranged from 1.0% to 7.0%. **Table 3** summarizes the investigated parameters and the selective parametric results with the yielding point (yielding load P_y and yielding displacement δ_y) being graphically defined in **Fig. 7**.

Regarding the naming regime of the specimens in this study, it has four components. The first component indicates the tendon's materials including "C", "HC", "A", "B", "G", and "S" which respectively stand for commonly-used CFRP, high-modulus CFRP, AFRP, BFRP, GFRP, and steel tendons. The second component is about the span-to-depth ratio (L/d_p), e.g.

L11 for L/d_p = 11, L16 for L/d_p = 16, and L20 for L/d_p = 20. The next component represents the ratio of the position of deviators to the beam's span (L_d/L), which includes Ex17 (L_d/L = 0.17), Ex33 (L_d/L = 0.33), and Ex47 (L_d/L = 0.47). However, if the third component is "In", it indicates that the beam is prestressed with internal tendons. Lastly, the reinforcing index (ω) is exhibited in the final component: r10 for ω = 1.0%, r17 for ω = 1.7%, r35 for ω = 3.5%, and r70 for ω = 7.0%. Take beam C-L11-Ex17-r17 as an example, this beam was post-tensioned with external commonly-used CFRP tendons with a span-to-depth ratio L/d_p = 11, the position of deviators L_d/L = 0.17 and a reinforcing index ω = 1.7%.

3.1. *Influence of the position of deviators (L_d/L) and reinforcing index (ω)*

The effects of the position of the deviators (L_d/L) and reinforcing index (ω) on the flexural behavior of dry key-jointed PSCBs post-tensioned with CFRP tendons are shown in **Fig. 8**, in which two beam groups are illustrated. The first group was PSCBs with ω = 1.7% containing most of the beams with tension-controlled failure while the second group contained compression-controlled PSCBs with ω = 3.5%. It means that the parametric analysis in this study covered a wide range of the behavior of PSCBs. The loading resistance of the tension-controlled beams was governed by the failure of prestressing tendons whereas concrete failure without the prestressing tendons rupture or yielding was the failure mode of the compression-controlled beams. In each group, there were four beams including one PSCB with internal unbonded tendons which served as a reference beam (with "In" in the third part of the beam's name), and three PSCBs with external tendons with the ratio of L_d/L = 0.17, 0.33 and 0.47, respectively. It is worth mentioning that L_d = 1700 (L_d/L = 0.47) is the maximum L_d that can be achieved for the beam's configuration in this parametric study (**Fig. 6**) since it is not practically feasible to place a deviator at the middle joint.

The bending behavior of PSCBs prestressed with internal or external tendons comprised two phases which were separated by a transition phase when the joint was opening (**Fig. 8)**. The beams responded elastically in the first phase before the joint opening and afterward they behaved in an inelastic manner until failure with the joint opening causing a reduction in the beam's stiffness and a more rapid gain in the beam's displacement and tendon stress (**Figs. 8a** and **b**). It is worth noting that the tendon stress increase is the tendon stress caused by the applied loads. The total stress in tendons is the sum of the initial effective prestressing stress (f_{pe}) and the tendon stress increase. Also, the maximum deflection of both tension- and compression-controlled PSBCs in **Fig. 8** (75-161 mm) was significantly greater than the serviceability limit of $L/800$ (= 4.5 mm) according to AASHTO LRFD [50]. Therefore, it can be inferred that using external CFRP tendons can offer PSBCs sufficient warning before the structure reaches its ultimate stage.

It is evident that the second-order effect was negligible in the first elastic phase before the joint opening since the behaviors of PSCBs with internal and external tendons were almost the same (**Figs. 8a** and **b**). A similar observation was also reported in the previous studies on monolithic beams externally prestressed with unbonded steel tendons [8, 39, 51]. It is understandable because the beam's displacement was still small and therefore the reduction in the tendon's depth compared to its initial depth (d_p) in the PSCBs with external tendons was marginal in the first phase as shown in **Fig. 8c**, in which d_p and d_{pe} are respectively the depth of the external tendons when the beam is not loaded and when the beam is loaded, and d_{pe} is called as the effective depth of external tendons. For example, as shown in **Table 3**, the effective depth of the tendons at the yielding point (d_{py}) of the PSCBs with external tendons and ω = 1.7% (beam C-L16-Ex17-r17, C-L16-Ex33-r17, and C-L16-Ex47-r17) was nearly equal to that of the reference PSCB with internal tendons (beam C-L16-In-r17). Thus, the yielding load (P_y) and displacement (δ_y) of those PSCBs with external tendons were similar to that of the reference PSCB with internal tendons with the variation not exceeding 4% (**Table 3**). It should be noted that the transition phase of the PSCBs when the joint is opening can be represented by the yielding point (**Fig. 7**) or in other words, the yielding point can be the limit of the beam's elasticity over which the beam's behavior is inelastic.

Nonetheless, as the beam's displacement increased at a faster rate after the joint opening (**Fig. 8a**) and so did the reduction in the tendon's effective depth (**Figs. 8c** and **d**), the second-order effect became pronounced accordingly. Due to the second-order effect, the stiffness, tendon stress increase, and loading resistance of the PSCBs with external tendons were lower than those of the reference PSCBs with internal tendons, especially in the PSCBs with a small L_d/L ratio (**Figs. 8a** and **b**). Also, it can be seen that the second-order effect tended to diminish when the position of deviators approached the middle joint of the PSCBs. For example, at the ultimate stage, when L_d/L ratio increased from 0.17 to 0.47 in the PSCBs with ω = 1.7%, the ratio of the tendon's effective depth of the PSCBs with external tendons ($d_{pu,Ex}$) to the tendon's effective depth in the reference PSCB with internal tendons ($d_{p,In}$) increased from 0.54 to 0.98 (**Fig. 9a**). In other words, the external tendon's effective depth was approaching the corresponding internal tendon's effective depth when L_d/L was close to 0.5. As a result, the reduction in the ultimate tendon stress and loading resistance of the PSCBs with external tendons compared to internal tendons decreased (**Figs. 9b** and **c**), e.g. the ultimate tendon stress and loading resistance of the PSCB with external tendons for the case with L_d/L = 0.47 and ω = 1.7% were just respectively 2% and 5% smaller than that of the reference PSCB with internal tendons (**Figs. 9b** and **c**). Meanwhile, the ductility of the PSCBs with external tendons slightly decreased when increasing the L_d/L ratio as shown in **Fig. 9d**. The ratio of the ductility index ($\mu = \delta_u/\delta_y$) of the PSCBs with external tendons to that with internal tendons changed from 1.05 to 0.93 when the L_d/L ratio increased from 0.17 to 0.47 (**Fig. 9d**). Furthermore, from the results in **Fig. 8**a, it can be deduced that the position of deviators plays a significant role in the failure mode of PSCBs with external tendons, i.e. decreasing L_d/L can change the failure mode from tension-controlled to compression-controlled. Therefore, the position of deviators should be taken into consideration when deriving the formula to determine the balanced reinforcement ratio for PSCBs with external tendons which has not yet been available in the open literature. Regarding the influence of the reinforcing index ω, increasing ω improved the yielding load P_y and loading resistance P_u but reduced the ductility of the PSCBs with external tendons. As ω increased from 1.7% to 3.5%, P_y and P_u of the PSCBs (ω = 3.5%) were respectively 1.8 and 2.3 times higher than those of PSCBs with ω = 1.7% (**Table 3**). However, since the PSCBs' behavior changed from tension-controlled to compression-controlled when increasing ω from 1.7% to 3.5% (**Fig. 8a**), the ductility index significantly reduced from 89-101 to 25-28 (**Table 3**). Also, it is evident from **Fig. 9** that increasing ω mitigated the second-order effect at the ultimate stage. As ω increased from 1.7% to 3.5%, the reduction in the external tendon's effective depth at the ultimate stage regarding its initial depth became smaller (**Fig. 9a**), which reduced the second-order effect in the PSCBs as shown in **Figs. 9b** and **c**. The smaller reduction of the external tendon's ultimate effective depth regarding its initial depth can be attributed to the decrease in the ultimate displacement of the beams when increasing ω as shown in **Fig. 8d**. Therefore, it can be deduced that the second-order effect is proportionate to the displacement of the beams. Moreover, as mentioned previously, due to the harping/bending effect at deviators, the ultimate tendon stress at the outermost fiber ($f_{pu,out}$) was higher than that at the central fiber ($f_{pu,cen}$) (**Table 3**). When increasing ω, the variation between $f_{pu,out}$ and $f_{pu,cen}$ became smaller (**Fig. 10**), which implies that the harping effect at deviators is mitigated if the PSCBs use a high ω. The harping effect is proportionate to the bending angle of the tendons at the deviators [35, 36], and the harping angle (θ) increases with the displacement of the PSCB as depicted in **Fig. 11b**. Therefore, using a high ω, which reduced the ultimate displacement or ductility of the PSCBs (**Fig. 8a**), mitigated the harping effect at the deviators (**Fig. 10)**. Also, it appeared that L_d/L did not have a significant effect on the harping effect (**Fig. 10**).

Finally, in comparison with monolithic beams, the effect of L_d/L on the loading resistance of PSCBs was found to be different. As observed in the previous analytical studies on the simply-supported monolithic beams prestressed with external tendons under two-point loading [8, 18], the optimal position of deviators to produce the highest loading resistance of the beam is within the loading points and midspan. However, in the case of PSCBs, the optimal position of deviators was at the midspan as mentioned earlier in this section. This can be explained by the difference in the bending shape at the ultimate stage between those types of beams, i.e. rectilinear rigid-body shape for segmental beams versus curvilinear shape for monolithic beams as shown in **Fig. 11**. It was found in the previous study by Tran et al. [16] that owing to the curvature concentrated at the middle joints (**Fig. 11d**), the bending shape of a PSCB at the ultimate stage is like two rigid bodies hinged by the top compressive concrete zone at the middle joint (**Fig. 11b**). Meanwhile, the bending deformation of the monolithic beam is uniformly distributed over the flexural span since its curvature distribution is not localized at the midspan (**Fig. 11h**) as in the case of the PSCB.

To be more precise, it is required to clarify how to determine the stress or strain of the tendons in a beam prestressed with external tendons because the loading resistance of the beam is primarily proportionate to the ultimate stress and the effective depth of the tendons (d_{pe} in **Fig. 11b**). The total elongation of unbonded tendons can be assumed equal to the total elongation of the concrete fiber at the tendon's level [18, 38]. The unbonded tendons are only anchored to the beam via the end anchorages, which implies that a whole member analysis is required to determine the tendon strain or stress [20, 23, 24], i.e. the strain of the unbonded tendons is determined by dividing the total elongation of the concrete at the tendon's level by the tendon's length between the anchorages. Also, the strain of a concrete fiber depends on the distance between this fiber and the neutral axis (z_{pe} in **Fig. 11b**) – that is, a concrete fiber with a higher z_{pe} has a higher strain. Therefore, the optimal position of the deviators to yield the highest stress and effective depth of an external tendon (or to eliminate the second-order effect) is the one producing the tendon's profile under loading as if the tendons were internal. In other words, the optimal deviator's position produces the smallest enclosed area between the deformed profile of internal and external tendons (the shaded area between the continuous line and dashed line in **Fig. 11b**) under the applied loads. In the case of a PSCB, when the deviators were close to the opening joints, the enclosed area between the deformed profile of internal and external tendons becomes smaller as shown in **Fig. 11c**. As a result, the optimal position of the deviators in PSCBs which offer the beam the highest strength is next to the opening joints, e.g. next to the middle joint in the PSCBs with the configuration used in this study. That is the reason why the second-order effect on the behavior of the PSCBs diminished significantly as previously observed when the L_d/L ratio approached 0.5. On the contrary, the enclosed area between the deformed profile of internal and external tendons becomes larger as the deviators move toward the midspan in a monolithic beam (**Fig. 11g**), which reduces the tendon stress and in turn the loading resistance of the monolithic beam. Also, it was found in the study by Harajli et al. [8] that when the deviators approach the midspan in the simply-supported monolithic beams under two-point loading, the premature failure of the beam happened under one of the loading points where the tendon's effective depth was smaller than that at midspan as illustrated in **Fig. 11g**.

3.2. *Influence of tendon's materials*

The effect of tendon's materials on the flexural behavior of PSCBs with external tendons is depicted in **Fig. 12**. Prior to the joint opening, the tendon's materials did not have an obvious effect on the beam's response. This is understandable because the PSCBs still remained their integrity when the joints were still closed under compression provided by the initial prestressing, and thus the concrete part dominated the stiffness of the PSCB's section [16]. After the joint opening, the tendons began to contribute more to the beam's stiffness as the area of compressive concrete decreased when the joint opened. Accordingly, Young's modulus of the tendons played a decisive role in the stiffness of the PSCBs, which meant that the PSCBs with the tendons having a higher Young's modulus had a higher bending stiffness (**Fig. 12a**). Also, using tendons with high Young's modulus provided the PSCBs with a high loading resistance (see **Fig. 12a** and **Table 3**). For example, with Young's modulus of CFRP tendons being approximately four-fold greater than that of GFRP tendons [145 GPa vs 39 GPa (**Table 1**)], the loading resistance of PSCBs increased by over two times when using CFRP tendons instead of GFRP tendons (beams C-L11-Ex33-r10 vs G-L11-Ex33-r10 in **Table 3**).

In comparison with steel tendons which have a plastic range in their behavior, the harping effect at the deviators, which causes high stress concentration in tendons, in a PSCBs prestressed with external FRP tendons can be more significant. For example, as shown in **Fig. 13**, the harping effect resulted in the ultimate FRP tendon stress at the outermost fiber 28-37% higher than that at the central fiber while the variation was just 7% in the case of the steel tendons due to the yielding of the steel tendons [the yield stress of the steel tendons is 1674 MPa (**Table 1**)]. However, as observed in **Fig. 14a**, apart from the high-modulus CFRP tendons (E_p = 200 GPa), the plastic-free behavior of the other types of FRP tendons, namely commonly-used CFRP (E_p = 145 GPa), AFRP, BFRP, and GFRP, did not reduce the ductility of the PSCBs since these FRP tendons all provided the PSCBs with comparable ductility to steel tendons. Despite the fact that the high-modulus CFRP tendons offered 16% more loading resistance for PSCBs compared to the steel tendons (**Fig. 14b**), the ductility of the PSCBs prestressed with the high-modulus CFRP tendons was significantly reduced by 33% compared to the steel tendons (**Fig. 14a**). It is noteworthy that the comparison about the ductility in this section was based on the behavior of tension-controlled PSCBs because in this type of beam the tendons govern the failure of the beam and thus the tendon's materials play a decisive role in the beam's ductility. In the case of compression-controlled PSCBs, owing to the failure mode being concrete crushing, the concrete governs the beam's ductility. Therefore, the ductility of a PSCB with high-modulus CFRP tendons and a PSCB with steel tendons with the same concrete material is expected to be similar.

From the results shown in **Figs. 12** and **14**, it can be concluded that of those types of FRP tendons investigated in this section, commonly-used CFRP tendons (E_p = 145 GPa) could be the most promising candidate to replace steel tendons in PSCBs prestressed with external tendons as the ductility and loading resistance of PSCBs using the commonly-used CFRP tendons were quite comparable to those using the steel tendons.

3.3. *Influence of span-to-depth ratio (L/d_p)*

The influence of the ratio of span-to-depth of the tendons (L/d_p) on the bending performance of PSCBs with external tendons is depicted in **Fig. 15**, in which d_p is the initial depth of the external tendons when the beam is not loaded. In this study, d_p was varied instead of L to maintain the location of the loading points and the joints. **Fig. 15** exhibits three beam groups with three different L/d_p (11, 16, and 20). In each group, there were two PSCBs: one beam was prestressed with external tendons with L_d/L = 0.33 and the other beam was prestressed with internal unbonded tendons acting as the reference for the second-order effect. All the PSCBs in **Fig. 15** had the same reinforcing index of ω = 1.7%. As seen in **Fig. 15**, L/d_p played a significant role in the flexural behavior of the PSCBs with external tendons. Since the sectional area of the beam was reduced when increasing L/d_p, the stiffness of the PSCBs became smaller, which resulted in the higher displacement of the beams under the same load (**Fig. 15a**). Increasing L/d_p also decreased yielding load P_y and loading resistance P_u of the PSCBs with external tendons considerably. For example, as L/d_p increased from 11 to 20, there were reductions of 80% and 83% in P_y and P_u of the PSCB (beam C-20-Ex33-r17 vs C-11-Ex33-r17 in **Table 3**), respectively. On the other hand, the PSCBs became more ductile when L/d_p rose as the ductility index (μ) of beam C-20-Ex33-r17 was more than twice higher than that of beam C-11-Ex33-r17 (**Table 3**).

$$R_d = \frac{d_{pe}}{d_p} = \frac{d_p - \left(\delta_{mid} - \delta_{dev}\right)}{d_p} = \frac{d_p - \delta_{mid}\left(1 - 2L_d / L\right)}{d_p} = 1 - k_1 \frac{\delta_{mid}}{d_p} \tag{11}$$

Meanwhile, the second-order effect became more significant when L/d_p increased (**Fig. 15b, c,** and **d**). Given the same displacement, the external tendon's effective depth reduced when increasing L/d_p as shown via the ratio of d_{pe}/d_p being reduced in **Fig. 15b**. This can be explained by considering the tendon's depth reduction factor R_d in **Eq. (11)** shown below, where δ_{dev} is the displacement of the deviators and equal to $2L_d/L\times\delta_{mid}$ based on the rectilinear bending shape of the PSCB (**Fig. 11b**), and k_1 is a factor depending on the position of the deviators and the bending shape of the beam and with the configuration of the PSCBs used in this parametric study (**Fig. 6**), $k_1 = 1 - 2L_d/L$. According to **Eq. (11)**, under the same displacement, increasing L/d_p (or reducing d_p) reduces R_d or in other words, the external tendon's effective depth decreases when L/d_p increases. Moreover, due to the higher ultimate displacement of the PSCBs with higher L/d_p (**Fig. 15a**), the second-order effect was more pronounced in these PSCBs. As L/d_p increased from 11 to 20, at the ultimate stage, the ratio of the tendon's effective depth in the PSCBs prestressed with external tendons ($d_{pu,Ex}$) to the effective depth of the internal tendons in the reference PSCBs ($d_{p,In}$) decreased from 0.90 to 0.66 (**Fig. 15c**). This reduction implied that the reduction of the external tendon's depth due to the second-order effect was amplified when L/d_p increased. Consequently, the reduction of the loading resistance of PSCBs with external tendons compared to the reference PSCBs with internal tendons increased from 16% to 47% when L/d_p increased from 11 to 20 (**Fig. 15d**). Lastly, as discussed in section 3.1, the harping effect is proportionate to the displacement of the beam. As a result, increasing L/d_p, which increased the displacement of the PSCBs, intensified the harping effect as illustrated in **Fig. 16**.

4. ANALYTICAL EVALUATION

This section is devoted to verifying the accuracy of some available models to estimate the effective depth (d_{pu}) and stress (f_{pu}) of external FRP tendons at the ultimate stage of PSCBs. The verification is conducted by using the numerical results on PSCBs in this study and it covers a wide range of primary parameters including the distance of deviators, effective prestressing level, prestressing reinforcement ratio, span-to-depth ratio, and material properties of FRP tendons. The models which are not deemed complicated and tedious for the design purpose, e.g. not involving a long iterative procedure, are reviewed in this section.

4.1. *Effective depth of external tendons at the ultimate stage (d_{pu})*

Mutsuyoshi et al. [52] proposed **Eq. (12)** to predict the ultimate effective depth of an external tendon (d_{pu}) in a simply-supported beam with two deviators under two-point loading:

$$d_{pu} = d_p \left[1.0 - 0.022 \left(\frac{L}{d_p} - 5.0 \right) \times \left(\frac{S_d}{L} - 0.2 \right) \right] \tag{12}$$

where d_p is the initial depth of the tendons when the beam is not loaded, L is the beam's span, $S_d = L\text{-}2\times L_d$ is the distance between the deviators, and L_d is the distance between the deviator and the nearest support (**Fig. 6**).

Aravinthan et al. [37] proposed **Eq. (13)** to predict d_{pu} in a simply-supported beam with two deviators under two-point loading and the model was adopted in ACI 440.4R-04 [24].

$$d_{pu} = d_p \left(1.25 - 0.01 \times \frac{L}{d_p} - 0.38 \times \frac{S_d}{L} \right) \leq d_p \tag{13}$$

He and Liu [18] also suggested an equation to estimate d_{pu} in a simply-supported beam with two deviators under two-point loading, which is expressed as follows:

$$d_{pu} = d_p \left(1.0 - 0.012 k_1 \frac{L}{d_p} \right) \tag{14}$$

where k_1 is a parameter accounting for the loss of the eccentricity of tendons and depending on the position of the deviators, types of loading, and the bending shape of the beam. For the configuration of the PSCBs used in this study (**Fig. 6**), k_1 = 1- $2L_d/L$.

Fig. 17 compares the numerical results and analytical predictions of d_{pu}. All the models yield unconservative prediction of d_{pu} in PSCBs. For example, the mean values of prediction-to-simulation ratios of the models by Mutsuyoshi et al. [52], Aravinthan et al. [37], and He and Liu [18] were 1.14, 1.12, and 1.15, respectively (**Fig. 17**). All three models were based on monolithic structures and therefore the difference in the flexural behavior between the segmental beams and monolithic beams as discussed previously could be the reason for the unconservative predictions. Among the three models, the model proposed by Aravinthan et al. [37] was the most accurate as it yielded the lowest mean and COV values which were 1.12 and 0.16, respectively (**Fig. 17**).

4.2. *Ultimate stress of external tendons (f_{pu})*

Mutsuyoshi et al. [52] proposed **Eqs. (15)** and **(16)** to estimate the ultimate stress of an external tendon (f_{pu}) in a simply-supported beam with two deviators under two-point loading:

$$f_{pu}\ (\text{MPa}) = f_{pe} + \Delta f_{pu} = f_{pe} + \Omega_u E_p \varepsilon_{cu}\left(\frac{d_{pu}}{c_u} - 1\right) \tag{15}$$

$$\Omega_u = \frac{\left(1.47 + 10.3 \times S_L / L\right)}{L / d_p} - 0.29 \times \frac{S_L}{L} \times \frac{S_d}{d_p} \tag{16}$$

where Ω_u is a bond reduction factor, E_p (MPa) is the tendon's modulus of elasticity, ε_{cu} = 0.003 is the ultimate strain of concrete, d_{pu} (mm) is the effective depth of the external tendon at the ultimate stage and determined by **Eq. (12)**, c_u is the depth of the neutral axis at the ultimate stage, d_p is the initial depth of the external tendon when the beam is not loaded, S_L and S_d are respectively the distances between the loading points and between the deviators, and $S_d = L$-$2\times L_d$ (**Fig. 6**).

Aravinthan et al. [37] also proposed equations as given below to estimate f_{pu} in a simply-supported beam with two deviators under third-point loading:

$$f_{pu}\ (\text{MPa}) = f_{pe} + \Delta f_{pu} = f_{pe} + \Omega_u E_p \varepsilon_{cu} \left(\frac{d_{pu}}{c_u} - 1 \right) \quad (17)$$

$$\Omega_u = \frac{2.31}{L/d_p} + 0.21 \times \frac{A_{p,in}}{A_{p,tot}} + 0.06 \quad (18)$$

where Ω_u is a bond reduction factor, d_{pu} (mm) is the effective depth of the external tendon at the ultimate stage and determined by **Eq. (13)**, $A_{p,in}$ and $A_{p,tot}$ are respectively the area of internal bonded prestressing reinforcement and the total area of both internal and external prestressing reinforcement. **Eqs. (17)** and **(18)** were also adopted in ACI 440.4R-04 [24].

Ng [53] proposed the following formulas to predict the ultimate stress of an external tendon in a simply-supported beam with two deviators under two-point loading:

$$f_{pu}\ (\text{MPa}) = f_{pe} + \Delta f_{pu} = f_{pe} + \Omega_u E_p \varepsilon_{cu} \left(\frac{d_p}{c_u} - 1 \right) \quad (19)$$

$$\Omega_u = \left(0.895 - 1.364 \times \frac{L_L}{L} \right) \times \frac{d_p}{h} - k_s \quad (20)$$

$$k_s = \begin{cases} 0.0096 \times S_d / d_p & \text{for } S_d / d_p \le 15 \\ 0.144 & \text{for } S_d / d_p > 15 \end{cases} \quad (21)$$

where Ω_u is a bond reduction factor, L_L is the distance between the loading point and the nearest support (**Fig. 6**), h is the height of the beam's cross-section, and k_s is a constant taking into account the second-order effect.

In general, the previously mentioned models to determine f_{pu} have two components: effective prestressing stress (f_{pe}) + stress increase due to the applied loading (Δf_{pu}). Therefore, to evaluate the accuracy of the three models, a comparison between the analytical predictions and the numerical results is made on the tendon stress increase (Δf_{pu}) instead of f_{pu}. The comparison of Δf_{pu} between the numerical results and predictions by the models is shown in **Fig. 18**. Similar to the predictions of d_{pu}, the predictions of Δf_{pu} were unconservative in which the model of Aravinthan et al. [37] can be considered as the most accurate one among the three models evaluated in this section. The Mean and COV of the prediction-to-simulation ratios of the models by Mutsuyoshi et al. [52], Aravinthan et al. [37], and Ng [53] were respectively 1.55 and 0.22, 1.28 and 0.17, and 1.55 and 0.14 (**Fig. 18**). The unconservative predictions of the first two models could be attributed to the higher estimation of d_{pu} than the numerical model as mentioned previously (**Fig. 17**) while the unconservative predictions of the last model may be due to the use of the initial depth of external tendons (d_p) instead of the effective depth at the ultimate stage (d_{pu}). In addition, the error could also be due to the bond reduction factors in those models which were derived from the calibration with the data on monolithic structures.

From the foregoing assessment of the existing models to predict d_{pu} and f_{pu} of an external tendon, it can be deduced that the existing models which are created for monolithic structures are not suitable to be used in segmental structures because those models yield unconservative predictions. Hence, new models or modifications toward the existing models are sought for the more accurate estimation of d_{pu} and f_{pu} in PSCBs and they will be reported in a future study.

5. CONCLUSIONS

The flexural response of dry key-jointed PSCBs prestressed with external FRP tendons was comprehensively investigated in this study by using Abaqus/CAE [25]. The 3D FE models were successfully validated against the experiments reported in the literature. The validated models were then utilized to intensively study the effect of various parameters on the bending response of the PSCBs. Based on the findings, some conclusions can be drawn as follows:

1. The position of deviators has a negligible effect on the behavior of the PSCBs before the joint opening. After the joint opening, the second-order effect becomes significant but it can be mitigated if the deviators are located close to the joints which are likely

to open under certain loads due to the rectilinear rigid-body bending shape of the PSCB. Besides, the ductility is not significantly affected by the position of deviators.

2. Increasing the reinforcing index leads to an increase in the yielding load and loading resistance but a decrease in the ductility of PSCBs. The second-order effect on the beam's behavior and the harping effect on the tendon stress at deviators were both proportionate to the displacement of the beam. Thus, using a high reinforcing index could mitigate the second-order effect and the harping effect at the ultimate stage due to the beam's lower ultimate displacement.
3. Among different types of FRP tendons (commonly-used CFRP, high-modulus CFRP, AFRP, BFRP, and GFRP), commonly-used CFRP tendons (E_p = 145 GPa) are the optimal candidate to replace steel tendons in PSCBs prestressed with external tendons because they can offer comparable strength and ductility as steel tendons. Although high-modulus CFRP tendons (E_p = 200 GPa) improve the stiffness and strength of PSCBs, they can greatly reduce the beam's ductility.
4. Increasing the span-to-depth ratio reduces the stiffness, yielding load, and loading resistance but increases the ductility of PSCBs. Increasing the span-to-depth ratio also intensifies the second-order effect and harping effect at the ultimate stage due to the larger ultimate displacement of the beam.
5. The existing analytical models developed for monolithic beams were observed to produce unconservative predictions of the ultimate effective depth (d_{pu}) and stress (f_{pu}) of external tendons in PSCBs and therefore a new model or modifications to the existing models are needed for better predictions of d_{pu} and f_{pu}.

ACKNOWLEDGMENTS

The financial support from the Australian Research Council Laureate Fellowships FL180100196 is acknowledged.

DATA AVAILABILITY STATEMENT

All data, models, and code generated or used during the study appear in the published article.

REFERENCES

1. Muller, J., *Ten years of experience in precast segmental construction.* PCI J, 1975. **20**(1): p. 28-61.
2. Buyukozturk, O., M.M. Bakhoum, and S. Michael Beattie, *Shear behavior of joints in precast concrete segmental bridges.* J Struct Eng, 1990. **116**(12): p. 3380-3401.
3. Jiang, H., Q. Cao, A. Liu, T. Wang, and Y. Qiu, *Flexural behavior of precast concrete segmental beams with hybrid tendons and dry joints.* Constr Build Mater, 2016. **110**: p. 1-7.
4. Zhou, X., N. Mickleborough, and Z. Li, *Shear strength of joints in precast concrete segmental bridges.* ACI Struct J, 2005. **102**(1): p. 3.
5. Virlogeux, *External Prestressing*, in *IABSE Proceedings* 1982, International Association for Bridge and Structural Engineering: Zurich, Switzerland. p. 101-108.
6. Rabbat, B.G. and K. Sowlat, *Testing of segmental concrete girders with external tendons.* PCI J, 1987. **32**(2): p. 86-107.
7. Alkhairi, F.M. and A.E. Naaman, *Analysis of Beams Prestressed with Unbonded Internal or External Tendons.* J Struct Eng, 1993. **119**(9): p. 2680-2700.
8. Harajli, M., N. Khairallah, and H. Nassif, *Externally prestressed members: evaluation of second-order effects.* J Struct Eng, 1999. **125**(10): p. 1151-1161.
9. Aparicio, A.C., G. Ramos, and J.R. Casas, *Testing of externally prestressed concrete beams.* Eng Struct, 2002. **24**(1): p. 73-84.
10. Yuan, A., Y. He, H. Dai, and L. Cheng, *Experimental Study of Precast Segmental Bridge Box Girders with External Unbonded and Internal Bonded Posttensioning under Monotonic Vertical Loading.* J Bridge Eng, 2015. **20**(4).
11. Le, T.D., T.M. Pham, H. Hao, and H. Li, *Behavior of Precast Segmental Concrete Beams Prestressed with External Steel and CFRP Tendons.* J Compos Constr, 2020. **24**(5): p. 04020053.
12. Woodward, R. and F. Williams, *COLLAPSE OF YNS-Y-GWAS BRIDGE, GLAMORGAN.* Proc Inst Civ Eng, 1988. **84**(4): p. 635-669.
13. Wouters, J.P., K. Kesner, and R.W. Poston, *Tendon corrosion in precast segmental bridges.* Transp Res Rec, 1999. **1654**(1): p. 128-132.
14. Le, T.D., T.M. Pham, H. Hao, and C. Yuan, *Performance of precast segmental concrete beams posttensioned with carbon fiber-reinforced polymer (CFRP) tendons.* Compos Struct, 2019. **208**: p. 56-69.
15. Le, T.D., T.M. Pham, and H. Hao, *Numerical study on the flexural performance of precast segmental concrete beams with unbonded internal steel tendons.* Constr Build Mater, 2020. **248**: p. 118362.
16. Tran, D.T., T.M. Pham, H. Hao, and W. Chen, *Numerical Investigation of Flexural Behaviours of Precast Segmental Concrete Beams Internally Post-tensioned with Unbonded FRP Tendons.* 2021. **(under review)**.
17. Harajli, M.H., *Strengthening of concrete beams by external prestressing.* PCI J, 1993. **38**(6): p. 76-88.
18. He, Z.-Q. and Z. Liu, *Stresses in external and internal unbonded tendons: Unified methodology and design equations.* J Struct Eng, 2010. **136**(9): p. 1055-1065.
19. Yuan, A., H. Dai, D. Sun, and J. Cai, *Behaviors of segmental concrete box beams with internal tendons and external tendons under bending.* Eng Struct, 2013. **48**: p. 623-634.

20. Nguyen-Minh, L., P. Phan-Vu, D. Tran-Thanh, Q. Phuong Thi Truong, T.M. Pham, C. Ngo-Huu, and M. Rovňák, *Flexural-strengthening efficiency of CFRP sheets for unbonded post-tensioned concrete T-beams.* Eng Struct, 2018. **166**: p. 1-15.
21. Truong, Q.P.T., P. Phan-Vu, D. Tran-Thanh, T.D. Dang, and L. Nguyen-Minh, *Flexural Behavior of Unbonded Post-Tensioned Concrete T-Beams Externally Bonded With CFRP Sheets Under Static Loading*, in *International Conference on Advances in Computational Mechanics 2017 (ACOME 2017). Lecture Notes in Mechanical Engineering*. 2018, Springer. p. 273-289.
22. Nguyen-Minh, L., D. Vo-Le, D. Tran-Thanh, T.M. Pham, C. Ho-Huu, and M. Rovňák, *Shear capacity of unbonded post-tensioned concrete T-beams strengthened with CFRP and GFRP U-wraps.* Compos Struct, 2018. **184**: p. 1011-1029.
23. Tran, D.T., P. Phan-Vu, T.M. Pham, T.D. Dang, and L. Nguyen-Minh, *Repeated and Post-Repeated Flexural Behavior of Unbonded Post-Tensioned Concrete T-Beams Strengthened with CFRP Sheets.* J Compos Constr, 2020. **24**(2): p. 04019064.
24. ACI, *Prestressing concrete structures with FRP tendons*, in *ACI 440.4R-04*. 2004, American Concrete Institute (ACI): Farmington Hills, Michigan.
25. Abaqus/CAE, *A general-purpose finite element software*. 2018, Dassault Systemes: France.
26. Carreira, D.J. and K.-H. Chu. *Stress-strain relationship for plain concrete in compression*. in *ACI J.* 1985.
27. Shahrooz, B.M., I.K. Ho, A.E. Aktan, R. de Borst, J. Blaauwendraad, C. van der Veen, R.H. Iding, and R.A. Miller, *Nonlinear Finite Element Analysis of Deteriorated RC Slab Bridge.* J Struct Eng, 1994. **120**(2): p. 422-440.
28. Birtel, V. and P. Mark, *Parameterised finite element modelling of RC beam shear failure*, in *ABAQUS Users' Conf.* 2006. p. 95-108.
29. Turmo, J., *Flexure and Shear Behaviour of Segmental Concrete Bridges with External Prestressing and Dry Joints*, in *ETSICCP de Barcelona. Dept. Ing. de la Construcción*. 2003.
30. Turmo, J., G. Ramos, and Á.C. Aparicio, *Shear behavior of unbonded post-tensioned segmental beams with dry joints.* ACI Mater J, 2006. **103**(3): p. 409-417.
31. Li, G., C. Zhang, and C. Niu, *Experimental study on shear behavior in negative moment regions of segmental externally prestressed concrete continuous beams.* J Bridge Eng, 2013. **18**(4): p. 328-338.
32. Jiang, H., Y. Li, A. Liu, Z.J. Ma, L. Chen, and Y. Chen, *Shear Behavior of Precast Concrete Segmental Beams with External Tendons.* J Bridge Eng, 2018. **23**(8).
33. Devalapura, R.K. and M.K. Tadros, *Stress-strain modeling of 270 ksi low-relaxation prestressing strands.* PCI J, 1992. **37**(2): p. 100-106.
34. Al-Mayah, A., K. Soudki, and A. Plumtree, *Novel anchor system for CFRP rod: Finite-element and mathematical models.* J Compos Constr, 2007. **11**(5): p. 469-476.
35. Quayle, T.G., *Tensile-flexural behaviour of carbon-fibre reinforced polymer (CFRP) prestressing tendons subjected to harped profiles*. 2005, University of Waterloo.
36. Grace, N.F. and G. Abdel-Sayed, *Behavior of externally draped CFRP tendons in prestressed concrete bridges.* PCI J, 1998. **43**(5).
37. Aravinthan, T., H. Mutsuyoshi, A. Fujioka, and Y. Hishiki, *Prediction of the Ultimate Flexural Strength of Externally Prestressed PC Beams.* Trans Jpn Concr Inst, 1997. **19**(2): p. 1233-1238.
38. Tam, A. and F. Pannell, *The ultimate moment of resistance of unbonded partially prestressed reinforced concrete beams.* Mag Concr Res, 1976. **28**(97): p. 203-208.
39. Alkhairi, F.M., *On the flexural behavior of concrete beams prestressed with unbonded internal and external tendons*. 1991, University of Michigan.
40. Moustafa, S.E., *Ultimate load test of a segmentally constructed prestressed concrete I-beam.* PCI J, 1974. **19**(4): p. 54-75.

41. MacGregor, R.J., M.E. Kreger, and J.E. Breen, *Strength and ductility of a three-span externally post-tensioned segmental box girder bridge model*. 1989, Center for Transportation Research, The University of Texas at Austin.
42. Rombach, G., *Precast segmental box girder bridges with external prestressing-design and construction.* INSA Rennes, 2002: p. 1-15.
43. Turmo, J., G. Ramos, and A.C. Aparicio, *FEM study on the structural behaviour of segmental concrete bridges with unbonded prestressing and dry joints: Simply supported bridges.* Eng Struct, 2005. **27**(11): p. 1652-1661.
44. Saibabu, S., V. Srinivas, S. Sasmal, N. Lakshmanan, and N.R. Iyer, *Performance evaluation of dry and epoxy jointed segmental prestressed box girders under monotonic and cyclic loading.* Constr Build Mater, 2013. **38**: p. 931-940.
45. Le, T.D., T.M. Pham, H. Hao, and Y. Hao, *Flexural behaviour of precast segmental concrete beams internally prestressed with unbonded CFRP tendons under four-point loading.* Eng Struct, 2018. **168**: p. 371-383.
46. Maissen, A. and C. de Smet, *Prestressed concrete using carbon fibre reinforced plastic (CFRP) strands.* Mater Struct, 1998. **31**(3): p. 175-177.
47. Zou, P.X., *Flexural behavior and deformability of fiber reinforced polymer prestressed concrete beams.* J Compos Constr, 2003. **7**(4): p. 275-284.
48. Wang, X., J. Shi, G. Wu, L. Yang, and Z. Wu, *Effectiveness of basalt FRP tendons for strengthening of RC beams through the external prestressing technique.* Eng Struct, 2015. **101**: p. 34-44.
49. ACI, *Building Code Requirements for Structural Concrete (ACI 318-19) and Commentary*, in *ACI 318-19*. 2019, American Concrete Institute (ACI): Farmington Hills, Michigan.
50. AASHTO, *AASHTO LFRP Bridge Design Specifications, 8th Edition*. 2017, American Association of State Highway and Transportation Officials (AASHTO): Washington, DC.
51. Tan, K.-H. and C.-K. Ng, *Effects of deviators and tendon configuration on behavior of externally prestressed beams.* ACI Struct J, 1997. **94**(1): p. 13-22.
52. Mutsuyoshi, H., K. Tsuchida, S. Matupayont, and A. Machida, *Flexural behavior and proposal of design equation for flexural strength of externally PC members.* Proc JSCE, 1995. **598**(26): p. 67-77.
53. Ng, C.K., *Tendon Stress and Flexural Strength of Externally Prestressed Beams.* ACI Struct J, 2003. **100**(5).
54. Sayed-Ahmed, E.Y. and N.G. Shrive, *A new steel anchorage system for post-tensioning applications using carbon fibre reinforced plastic tendons.* Can J Civ Eng, 1998. **25**(1): p. 113-127.
55. Kobraei, M., M.Z. Jumaat, and P. Shafigh, *An experimental study on shear reinforcement in RC beams using CFRP-bars.* Sci Res Essays, 2011. **6**(16): p. 3447-3460.
56. Wang, X., P. Xu, Z. Wu, and J. Shi, *A novel anchor method for multi-tendon FRP cable: Concept and FE study.* Compos Struct, 2015. **120**: p. 552-564.

NOTATION

c_u : neutral axis depth at ultimate, mm;

d_p : initial depth of tendons when the beam is not loaded, mm;

$d_{p,In}$: depth of tendons in PSCB with internal tendons, mm;

d_{pe} : effective depth of tendons under loading, mm;

d_{pu} : effective depth of tendons at the ultimate stage, mm;

$d_{pu,Ex}$: effective depth of tendons at ultimate in PSCBs with external tendons, mm;

d_{py} : effective depth of tendons at the yielding point, mm;

E_c : elastic modulus of concrete, N/mm^2;

E_p : Young's modulus of tendons, N/mm^2;

f'_c : concrete compressive strength, N/mm^2;

f_{ct} : concrete tensile strength, N/mm^2;

f_{pe} : effective prestressing stress, N/mm^2;

f_{pu} : tensile strength of tendons, N/mm^2;

$f_{pu,cen}$: tendon stress at the central fibre at ultimate, N/mm^2;

$f_{pu,in}$: tendon stress at the innermost fibre at ultimate, N/mm^2;

$f_{pu,out}$: tendon stress at the outermost fibre at ultimate, N/mm^2;

h : height of a beam, mm;

L : span of a beam, mm;

L_d : position of deviators with regard to the beam's supports, mm;

P_u : ultimate load or load-carrying capacity of a beam, kN;

P_y : yielding load, kN;

δ_{mid} : displacement at midspan, mm;

δ_{dev} : displacement at deviators, mm;

Δf_{pu} : ultimate stress increase of tendons, N/mm^2;

$\Delta_{joint,u}$: maximum joint opening, mm;

δ_u : ultimate displacement, mm;

δ_y : yielding displacement, mm;

ε_{cu} : ultimate concrete strain at the extreme compression fibre;

μ : ductility index, $= \delta_u/\delta_y$;

ρ_p : prestressing reinforcement ratio;

Ω_u : bond-reduction factor;

ω : reinforcing index, $= \rho_p \times f_{pe} / f'_c$;

LIST OF TABLES

Table 1. Material properties adopted in the parametric study

Concrete			
Mechanical properties		**CDP model's parameters** [a]	
Compressive strength f'_c (MPa)	44.0	Dilation angle ψ_{CDP} (degree)	30
Elastic modulus E_c (GPa)	31.17	Flow potential eccentricity ε	0.1
Poisson's ratio v	0.18	σ_{b0}/σ_{c0}	1.16
Tensile strength f_{ct} (MPa)	2.65	Second stress variant ratio K_c	0.667
		Viscosity parameter μ_{CDP}	0.001

Tendons and auxiliary steel reinforcements

	CFRP tendons	High-modulus CFRP tendons	AFRP tendons [b]	GFRP tendons [b]	BFRP tendons [d]	Steel tendons	Ø12	Ø10
Diameter (mm)							12	10
Area (mm^2)							113	78.5
Tensile strength (MPa)	2450 [a]	2400 [c]	1400	1080	1400	1860	587	538
(Nominal) yielding stress (MPa)						1674	534	489
Shear strength (MPa)	126 [a]		49	89				
Longitudinal tensile Young's modulus (GPa)	145 [a]	200 [c]	70	39	55	195	200	200
Transverse tensile Young's modulus (GPa)	10.3 [b]	10.3 [b]	5.5	8.6	8	195 [b]	200 [e]	200 [e]
Shear modulus (GPa)	7.2 [b]	7.2 [b]	2.2	3.8	6	73.1 [b]	77 [e]	77 [d]
Possion's ratio	0.27	0.27 [b]	0.35	0.28	0.3	0.3	0.3	0.3

Notes: [a] from the study by Le et al. [15], [b] from the study by Sayed-Ahmed and Shrive [54], [c] from the study by Kobraei et al. [55], [d] from the study by Wang et al. [56], [e] from the study by Al-Mayah et al. [34].

Table 2. Validation of numerical models

	C-D (external CFRP tendons) [11]			S-D (external steel tendons) [11]		
	Simulation	Experiment	Simu / Exp	Simulation	Experiment	Simu / Exp
P_u (kN)	104.8	109.0	0.96	86.4	86.3	1.00
δ_u (mm)	66.4	64.8	1.02	83.1	84.4	0.98
$\Delta_{joint,u}$ (mm)	25.6	26.9	0.95	32.6	34.4	0.95
At midspan						
$f_{pu,out}$ (MPa)	1811		0.95	1683*		1.01
$f_{pu,cen}$ (MPa)	1811	1898	0.95	1682*	1674*	1.00
$f_{pu,in}$ (MPa)	1810		0.95	1682*		1.00
At deviator						
$f_{pu,out}$ (MPa)	2114			1753		
$f_{pu,cen}$ (MPa)	1804			1647		
$f_{pu,in}$ (MPa)	1494			1541		

	D2 (external steel tendons) [9]			C3 (internal CFRP tendons) [14]		
	Simulation	Experiment	Simu / Exp	Simulation	Experiment	Simu / Exp
P_u (kN)	184.3	180.0	1.02	111.6	113.0	0.99
δ_u (mm)	103.5	100.0	1.04	100.9	95.0	1.06
$\Delta_{joint,u}$ (mm)	29.9	28.0	1.07	29.9	28.3	1.06
At midspan						
$f_{pu,out}$ (MPa)				2326		1.31
$f_{pu,cen}$ (MPa)	1648	1611	1.02	1913	1774	1.08
$f_{pu,in}$ (MPa)				1500		0.85
At deviator						
$f_{pu,out}$ (MPa)	1739					
$f_{pu,cen}$ (MPa)	1609					
$f_{pu,in}$ (MPa)	1478					

Notes: * at the maximum applied load.

Table 3. Selective results of the parametric analysis

Group	Beams	Tendon's materials	L/d_p	f_{pe}/f_{pu}	ρ_p	ω	L_d/L	d_{py} mm	P_y kN	δ_y mm	d_{pu} mm	P_u kN	δ_u mm	$\mu = \delta_u / \delta_y$	$f_{pu,out}$* MPa	$f_{pu,cen}$ MPa
1 & 2 Investigate L_d & ω	C-L16-In-r17	CFRP	16	0.3	0.10%	1.7%	In	226	13.9	1.5	226	39.6	148	96		1826
	C-L16-Ex17-r17	CFRP					0.17	225	14.0	1.6	122	15.9	161	101	2363	1610
	C-L16-Ex33-r17	CFRP					0.33	226	13.8	1.5	179	28.3	153	99	2450	1737
	C-L16-Ex47-r17	CFRP					0.47	226	13.9	1.6	222	37.8	141	89	2450	1786
	C-L16-In-r35	CFRP		0.35	0.18%	3.5%	In	226	32.9	3.2	226	54.2	81	25		1456
	C-L16-Ex17-r35	CFRP					0.17	225	32.3	2.9	174	37.4	82	28	1749	1383
	C-L16-Ex33-r35	CFRP					0.33	226	32.4	2.9	203	46.3	76	26	1738	1399
	C-L16-Ex47-r35	CFRP					0.47	226	32.6	3.0	224	53.1	75	25	1763	1430
3 Investigate L/d_p	C-L11-In-r17	CFRP	11	0.3	0.10%	1.7%	In	326	33.1	1.8	326	88.4	113	62		2011
	C-L11-Ex33-r17	CFRP					0.33	326	33.0	1.8	292	74.3	110	61	2450	1912
	C-L16-In-r17	CFRP	16				In	226	13.9	1.5	226	39.6	148	96		1826
	C-L16-Ex33-r17	CFRP					0.33	226	13.8	1.5	179	28.3	153	99	2450	1737
	C-L20-In-r17	CFRP	20				In	181	8.2	1.5	181	24.1	190	127		1855
	C-L20-Ex33-r17	CFRP					0.33	181	8.2	1.6	120	12.8	200	126	2383	1629
4 Investigate tendon's materials	S-L11-Ex33-r10	Steel	11	0.23	0.10%	1.0%	0.33	326	18.2	1.6	283	63.7	141	91	1789	1678
	C-L11-Ex33-r10	CFRP		0.18				326	18.6	1.5	285	68.0	134	89	2450	1794
	HC-L11-Ex33-r10	High-modulus CFRP		0.18				326	19.1	1.6	297	73.7	94	60	2400	1791
	A-L11-Ex33-r10	AFRP		0.31				326	18.0	1.4	287	44.6	127	88	1400	1086
	B-L11-Ex33-r10	BFRP		0.31				326	17.9	1.4	281	39.5	148	103	1361	1029
	G-L11-Ex33-r10	GFRP		0.40				326	17.8	1.4	281	32.5	147	102	1080	845

Notes: $f_{pu,out}$ and $f_{pu,cen}$ are the simulated ultimate tendon stress at the outermost and central fiber, respectively; * is located at the deviators.

Table 4. Effective depth and stress of the external tendons at ultimate from the simulation

No.	Beams	f'_c MPa	E_p GPa	f_{pu} MPa	L mm	d_p mm	L/d_p	L_d mm	L_d/L	f_{pe} MPa	ρ_p	ω	d_{pu} mm	$f_{pu,out}$ MPa	$f_{pu,cen}$ MPa	Δf_{pu} MPa
1	C-L11-Ex17-r17							600	**0.17**				250	2450	1873	1138
2	C-L11-Ex33-r17							1200	**0.33**	735	0.10%	**1.7%**	292	2450	1912	1177
3	C-L11-Ex47-r17							1700	**0.47**				323	2450	1924	1189
4	C-L11-Ex17-r35							600	**0.17**				290	1759	1448	590
5	C-L11-Ex33-r35	44	145	2450	3600	326	**11**	1200	**0.33**	858	0.18%	**3.5%**	309	1786	1473	615
6	C-L11-Ex47-r35							1700	**0.47**				325	1798	1508	650
7	C-L11-Ex17-r70							600	**0.17**				309	1674	1538	313
8	C-L11-Ex33-r70							1200	**0.33**	1225	0.25%	**7.0%**	318	1691	1550	325
9	C-L11-Ex47-r70							1700	**0.47**				326	1744	1571	346
10	C-L11-Ex33-r10		145	2450									285	2450	1794	1362
11	HC-L11-Ex33-r10		200	2400									297	2400	1791	1359
12	A-L11-Ex33-r10	44	70	1400	3600	326	**11**	1200	**0.33**	432	0.10%	**1.0%**	287	1400	1086	654
13	B-L11-Ex33-r10		55	1400									281	1361	1029	597
14	G-L11-Ex33-r10		39	1080									281	1080	845	413
15	C-L16-Ex17-r17							600	**0.17**				122	2363	1610	875
16	C-L16-Ex33-r17							1200	**0.33**	735	0.10%	**1.7%**	179	2450	1737	1002
17	C-L16-Ex47-r17							1700	**0.47**				222	2450	1786	1051
18	C-L16-Ex17-r35							600	**0.17**				174	1749	1383	525
19	C-L16-Ex33-r35	44	145	2450	3600	226	**16**	1200	**0.33**	858	0.18%	**3.5%**	203	1738	1399	541
20	C-L16-Ex47-r35							1700	**0.47**				224	1763	1430	572
21	C-L16-Ex17-r70							600	**0.17**				189	1917	1592	367
22	C-L16-Ex33-r70							1200	**0.33**	1225	0.25%	**7.0%**	211	1864	1581	356
23	C-L16-Ex47-r70							1700	**0.47**				225	1933	1612	387
24	C-L20-Ex17-r17							600	**0.17**				82	2106	1433	698
25	C-L20-Ex33-r17							1200	**0.33**	735	0.10%	**1.7%**	120	2383	1629	894
26	C-L20-Ex47-r17							1700	**0.47**				176	2447	1762	1027
27	C-L20-Ex17-r35							600	**0.17**				100	1938	1356	498
28	C-L20-Ex33-r35	44	145	2450	3600	181	**20**	1200	**0.33**	858	0.18%	**3.5%**	143	2034	1456	598
29	C-L20-Ex47-r35							1700	**0.47**				178	2060	1514	656
30	C-L20-Ex17-r70							600	**0.17**				137	1876	1577	352
31	C-L20-Ex33-r70							1200	**0.33**	1225	0.25%	**7.0%**	160	1913	1617	392
32	C-L20-Ex47-r70							1700	**0.47**				179	1964	1642	417

Notes: d_{pu} is the effective depth of the tendons at ultimate, $f_{pu,out}$ and $f_{pu,cen}$ are respectively the simulated ultimate tendon stress at the outermost and central fiber, Δf_{pu} is the ultimate tendon stress increase considered at the central fiber

LIST OF FIGURES

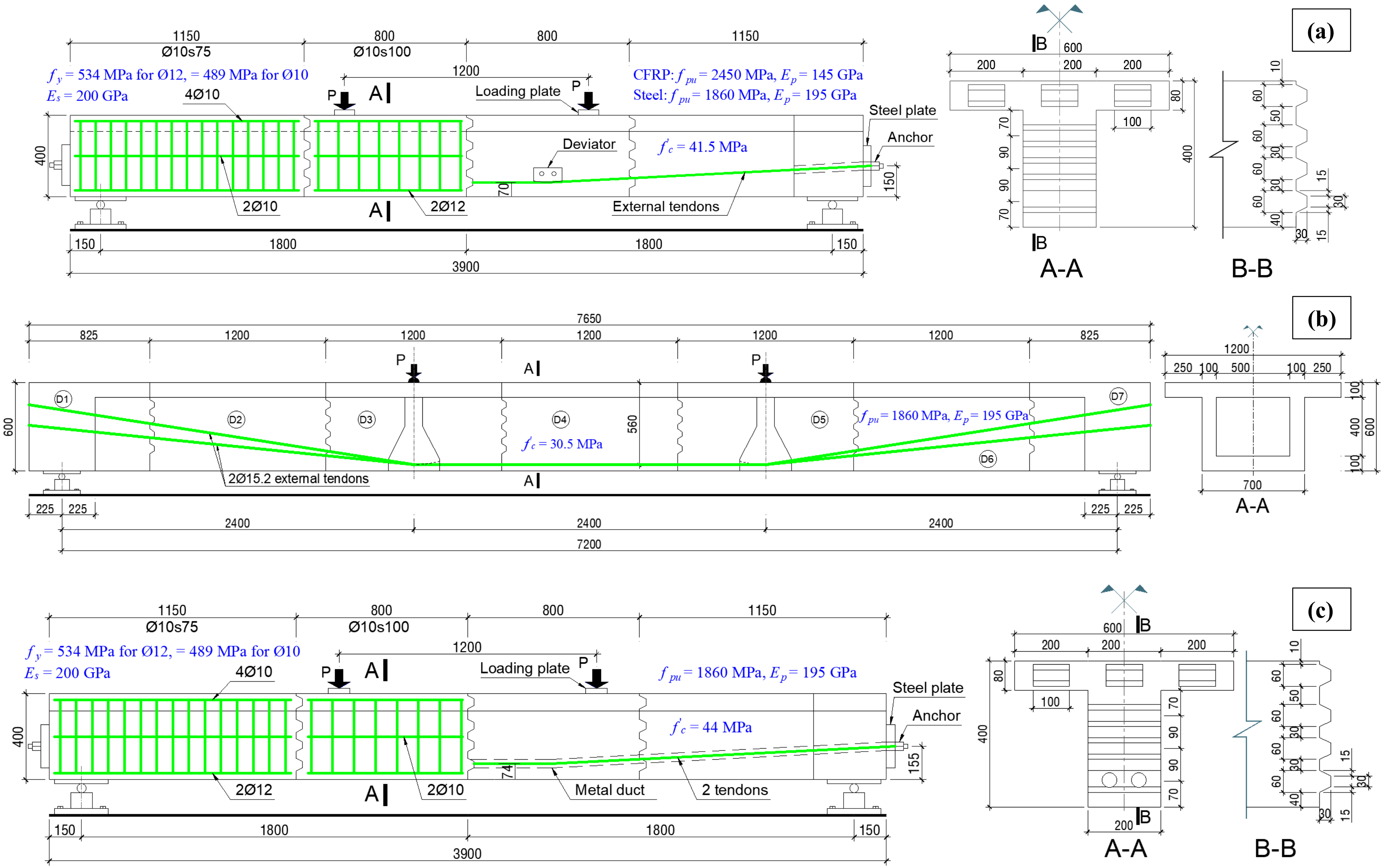

Fig. 1. Beam design: (a) C-D and S-D reported in [11], (b) D2 reported in [9], and (c) C3 reported in [14] (dimensions in mm)

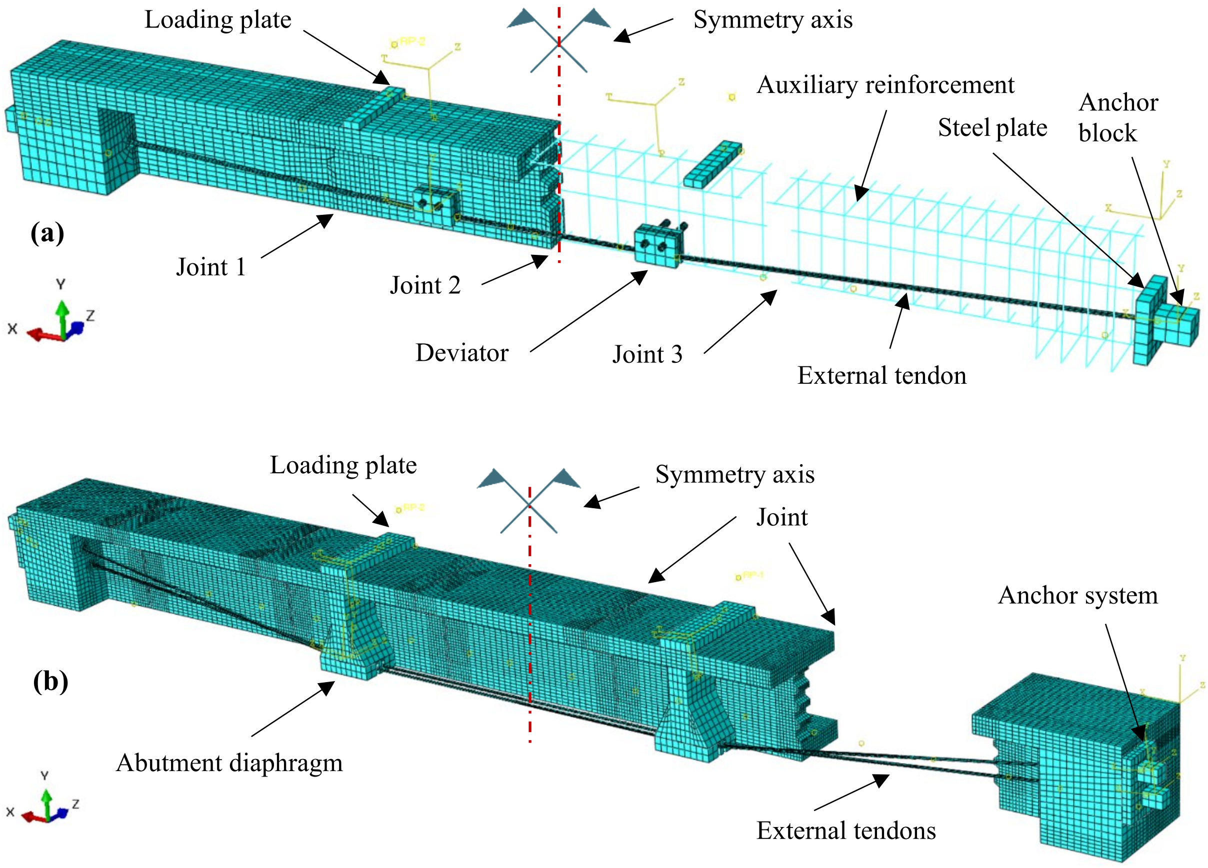

Fig. 2. A 3-D finite element model of a PSCB with external tendons: (a) T-section PSCB [11] and (b) box PSCB [9]

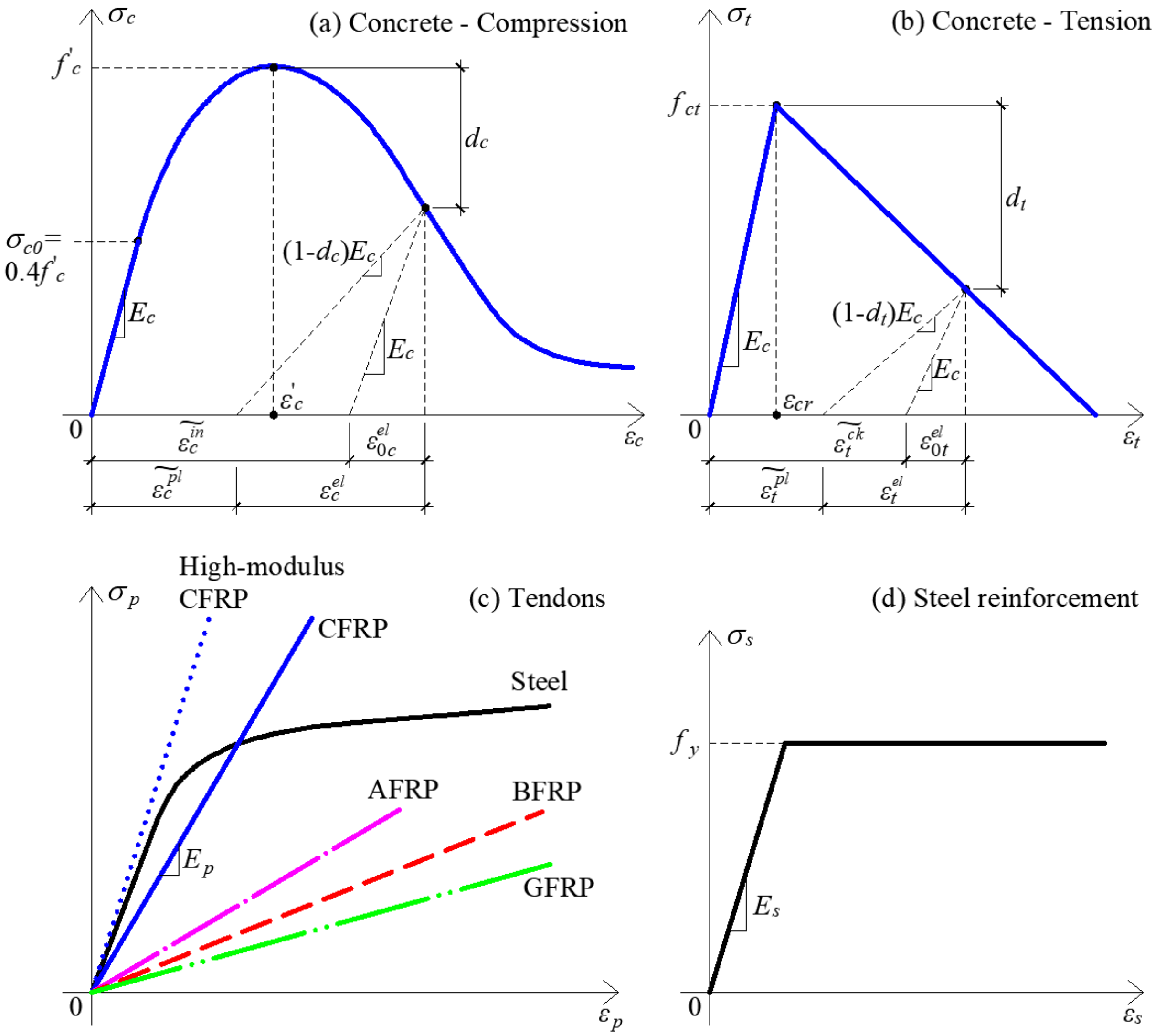

Fig. 3. Stress–strain relationships of the materials: (a) Concrete under compression, (b) Concrete under tension, (c) Tendons, and (d) Steel reinforcement

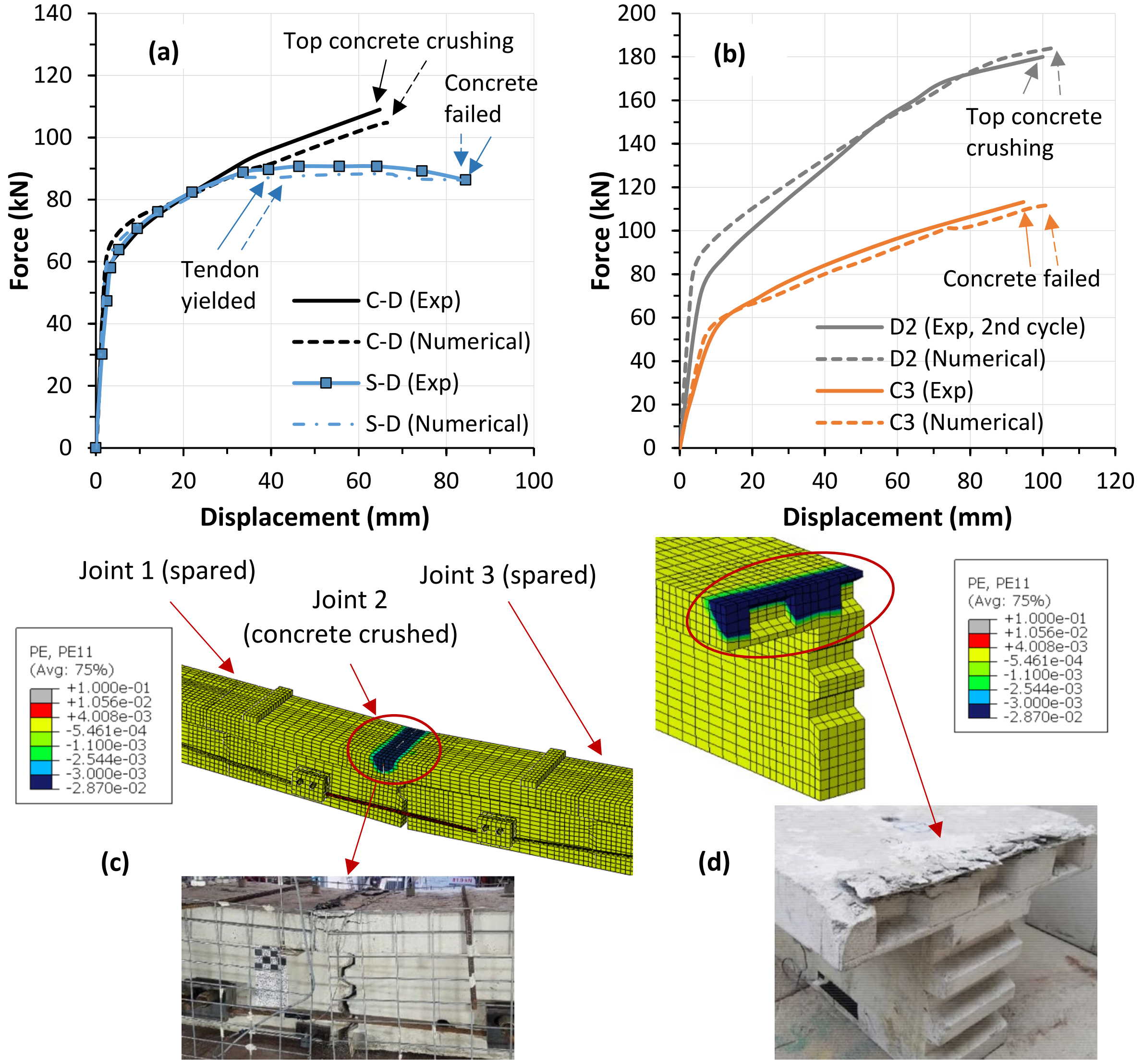

Fig. 4. Validation of the finite element model with the experimental results: (a) Beams C-D and S-D [11], (b) Beam D2 [9] and beam C3 [14], (c) Failure pattern of beam S-D, and (d) Failure pattern of beam C-D at its middle joint

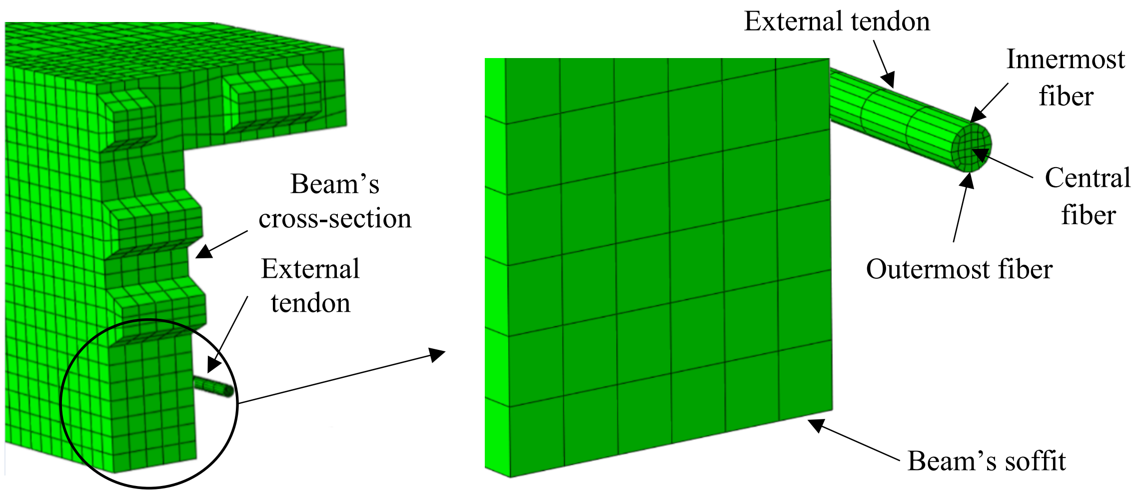

Fig. 5. Location of outermost, central and innermost fibers of the tendons

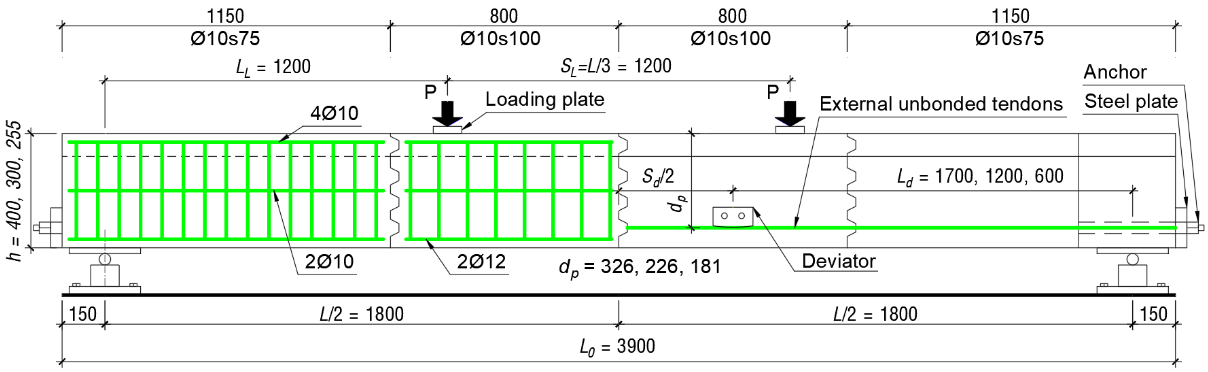

Fig. 6. Beam's configurations used in the parametric analysis (dimensions in mm)

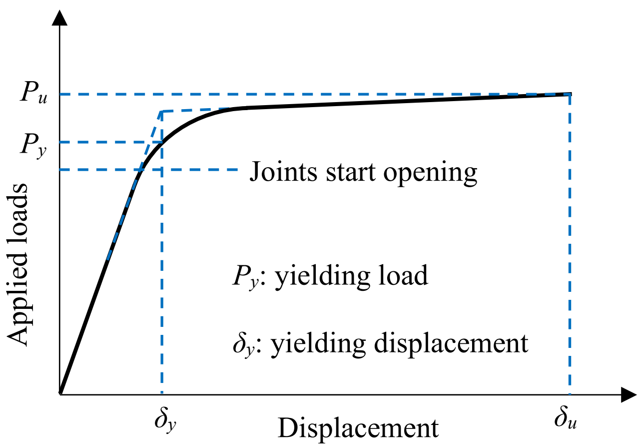

Fig. 7. Illustration of the yielding point

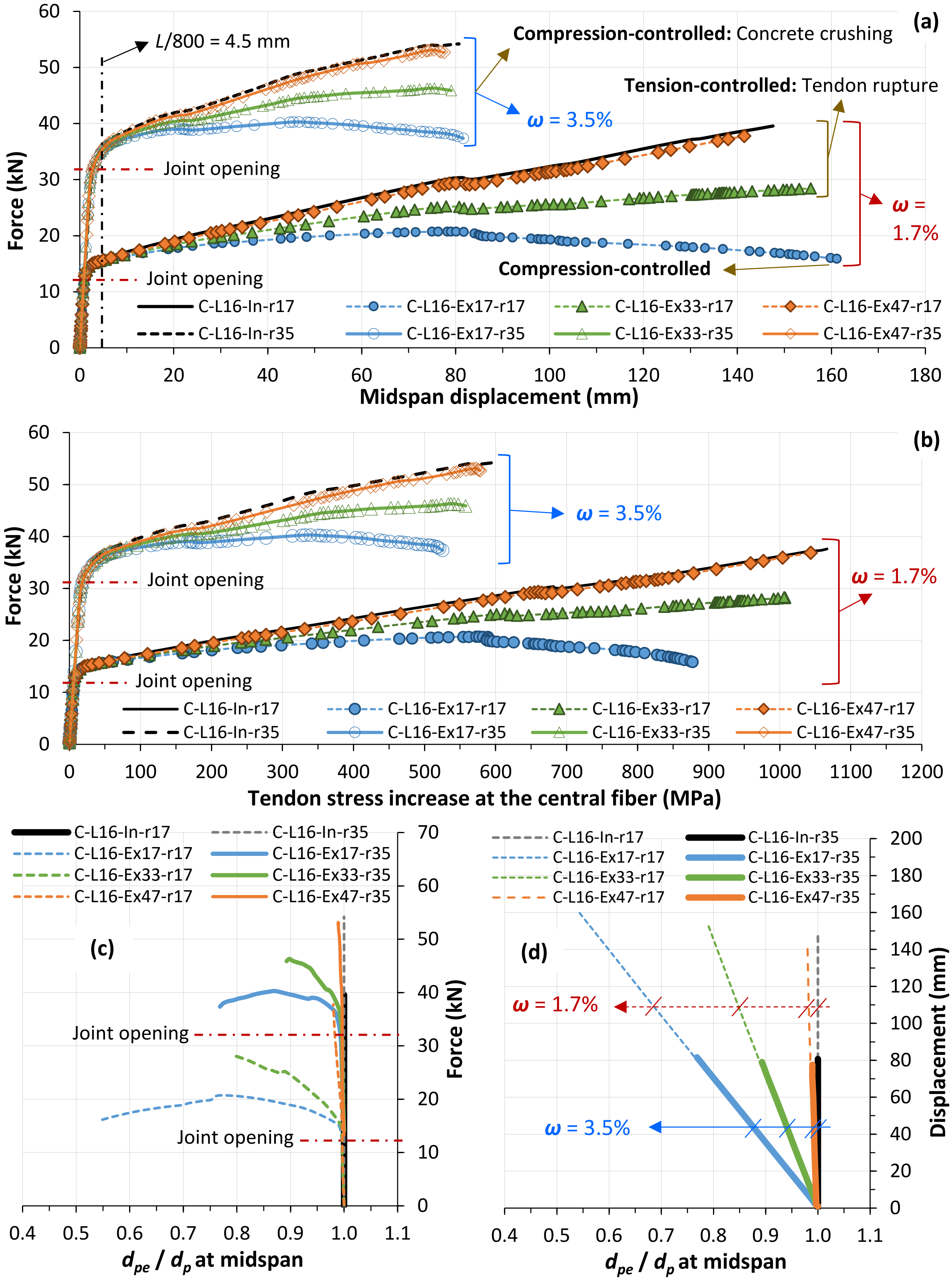

Fig. 8. Influence of the position of deviators (L_d) and reinforcing index (ω): (a) force-displacement curve, (b) force - tendon stress increase at midspan, (c) and (d) force and displacement - ratio of effective depth of tendon to its initial depth, respectively

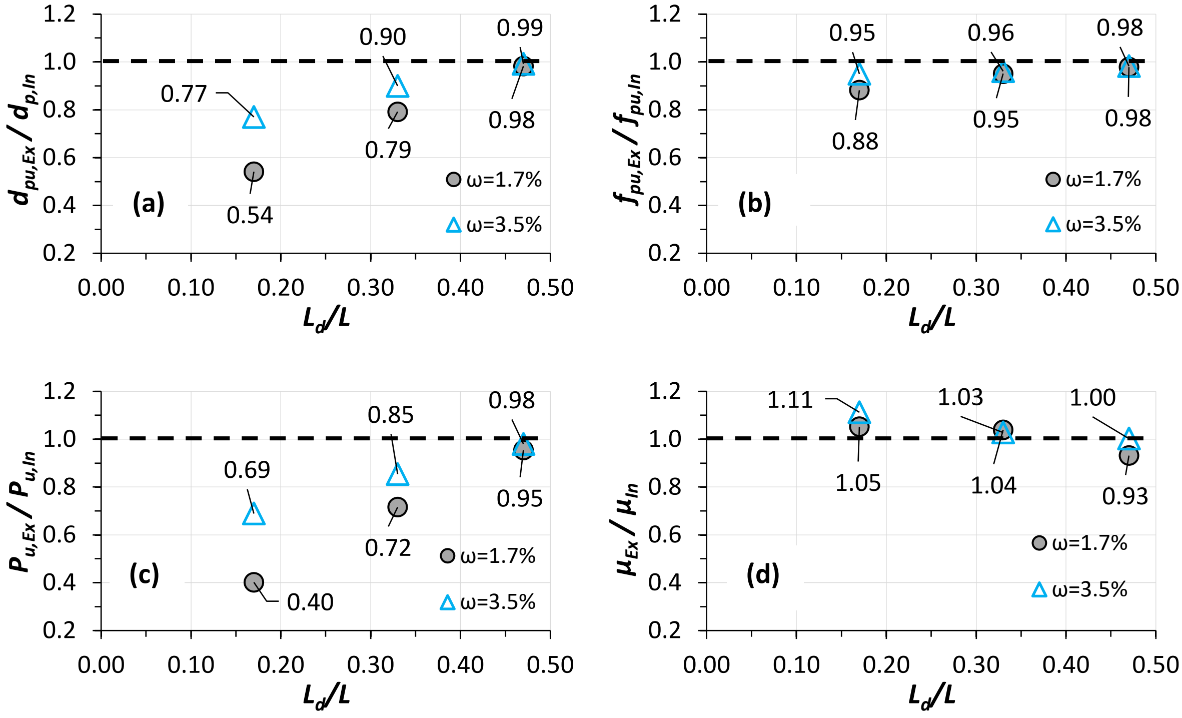

Fig. 9. External vs internal tendons at the ultimate stage of the PSCBs with L/d_p = 16: (a) effective depth of tendons (d_{pu}), (b) tendon stress (f_{pu}), (c) loading resistance (P_u), and (d) ductility index (μ)

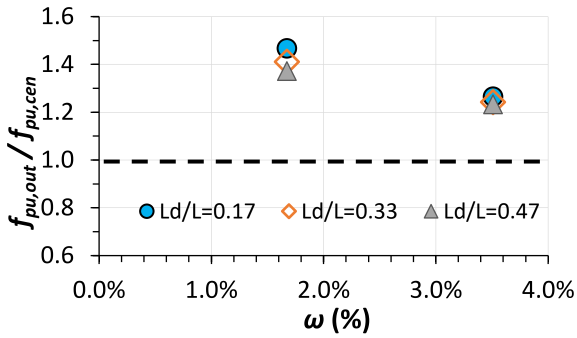

Fig. 10. Influence of ω and L_d/L on the harping effect

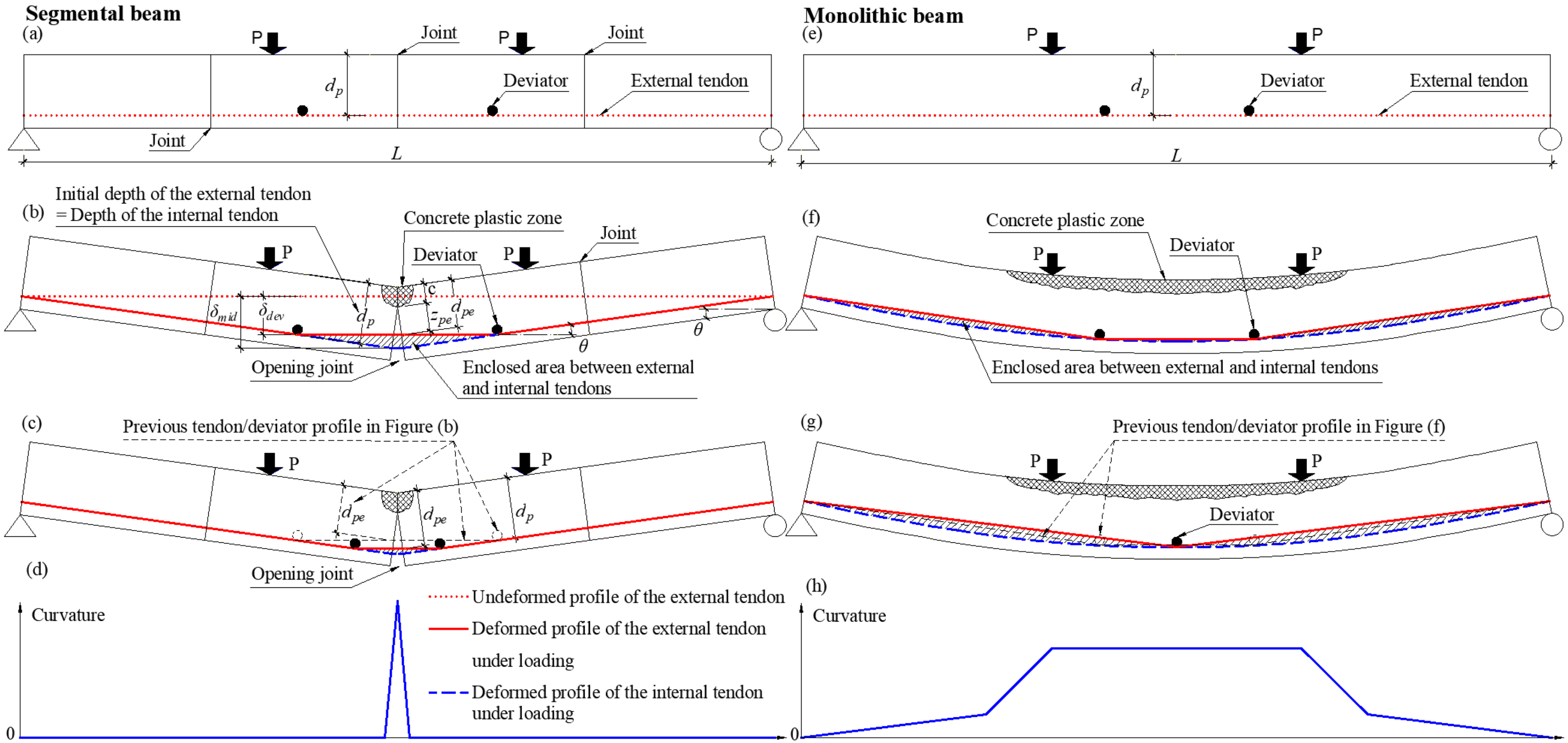

Fig. 11. Typical bending shapes of segmental and monolithic beams: (a) and (e) unloaded segmental and monolithic beams, respectively; (b) and (f) typical deflected geometry of segmental and monolithic beams, respectively; (c) and (g) deflected shape of segmental and monolithic beams when deviators approach midspan, respectively; (d) and (h) typical curvature distribution of segmental and monolithic beams, respectively

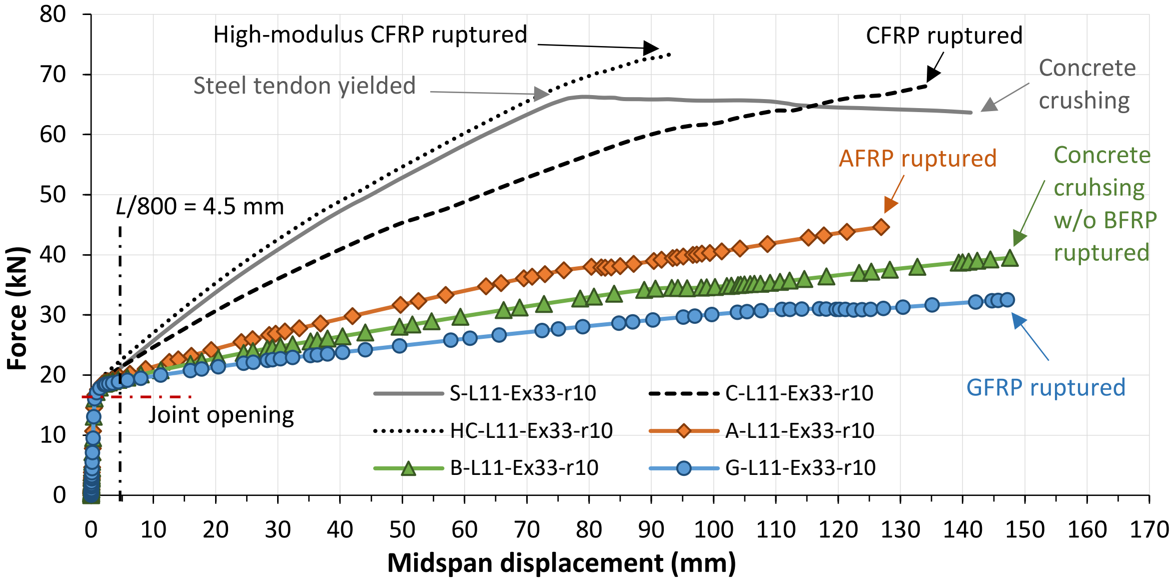

Fig. 12. Influence of tendon's materials on the force-displacement relationship

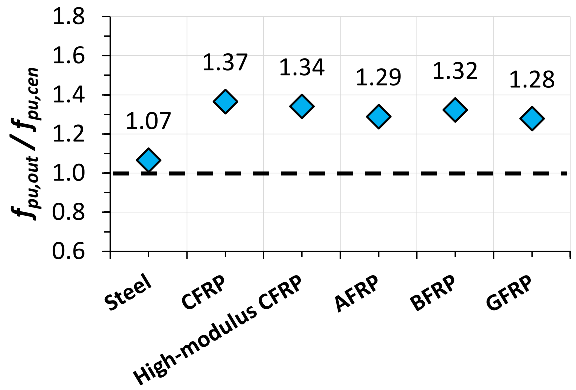

Fig. 13. Influence of tendon's materials on the harping effect

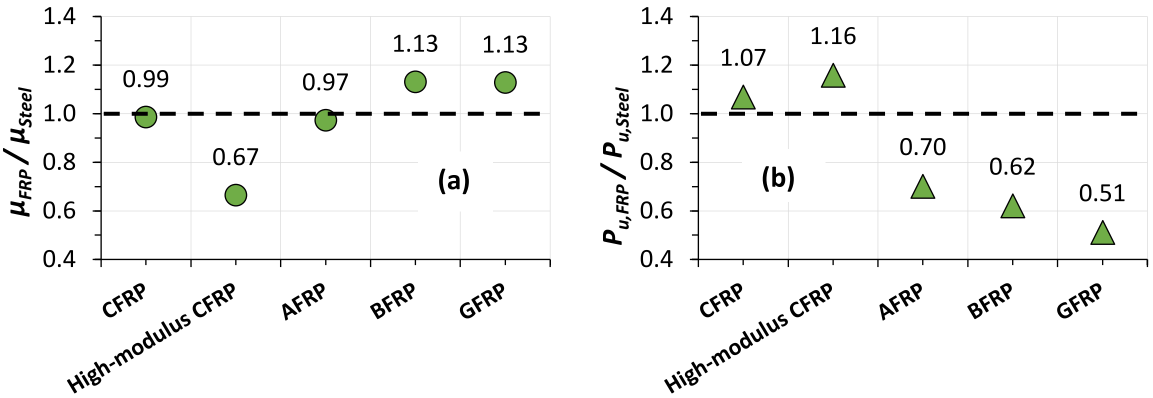

Fig. 14. FRP vs steel tendons: (a) ductility index (μ) and (b) loading resistance (P_u)

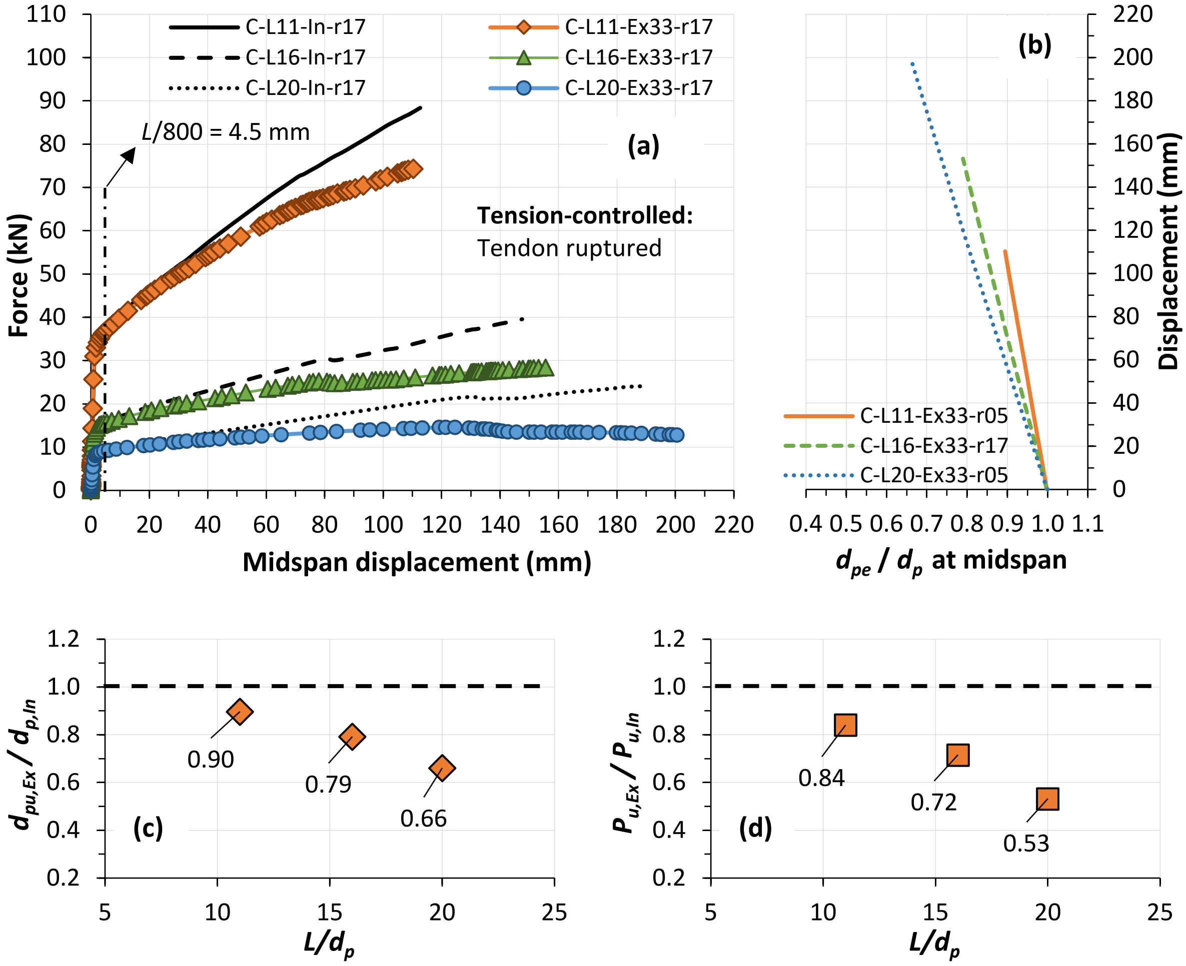

Fig. 15. Influence of span-to-depth ratio (L/d_p): (a) force-displacement, (b) displacement-effective depth of tendons relationship, and external vs internal tendons at the ultimate stage in terms of (c) tendon's effective depth (d_{pu}) and (d) loading resistance (P_u)

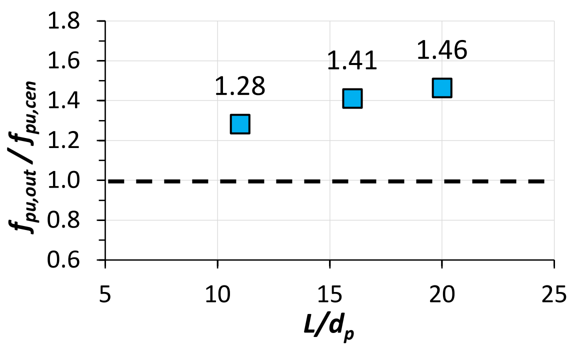

Fig. 16. Influence of L/d_p on the harping effect

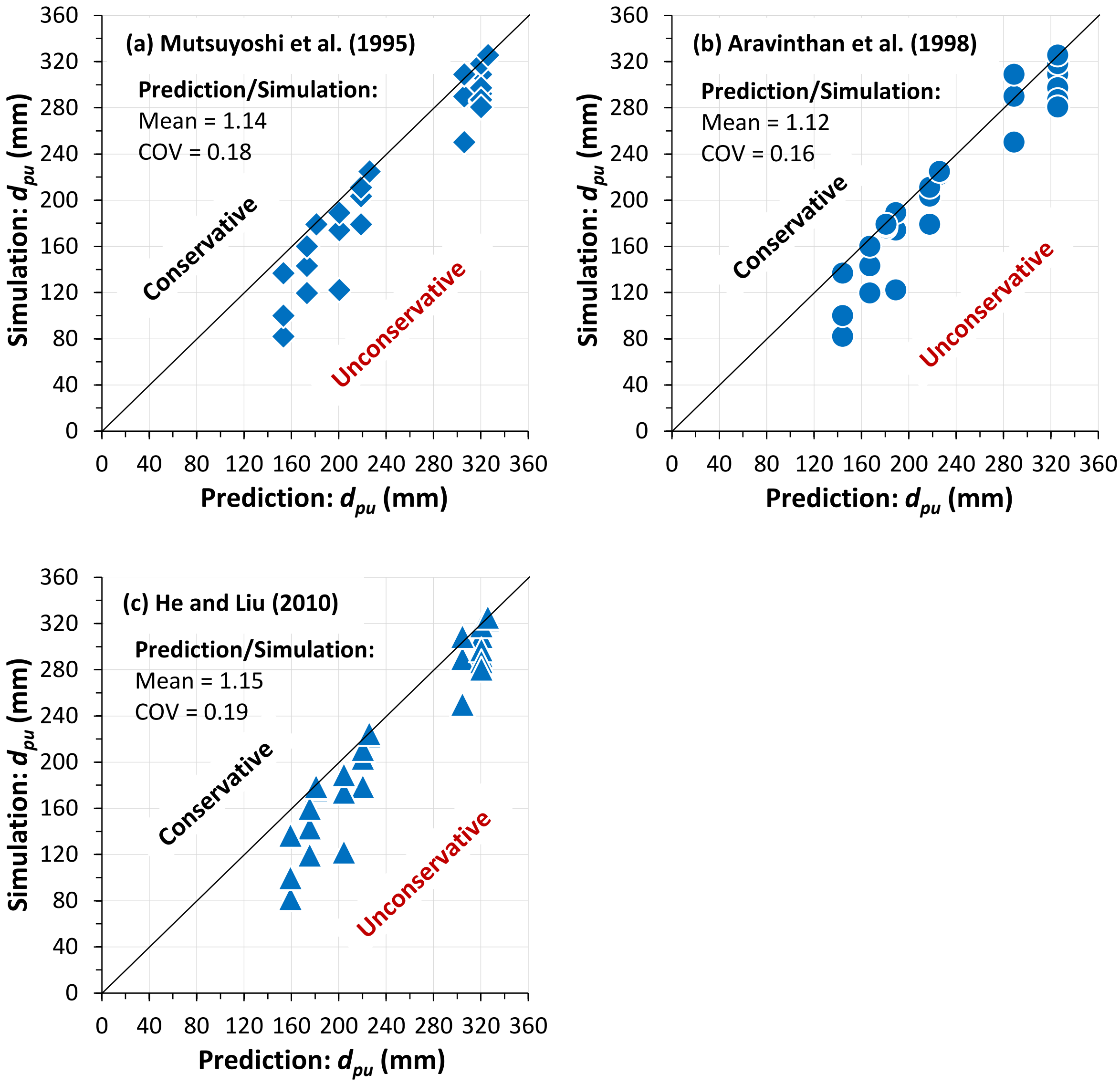

Fig. 17. Effective depth of external tendons at ultimate: predictions vs simulation

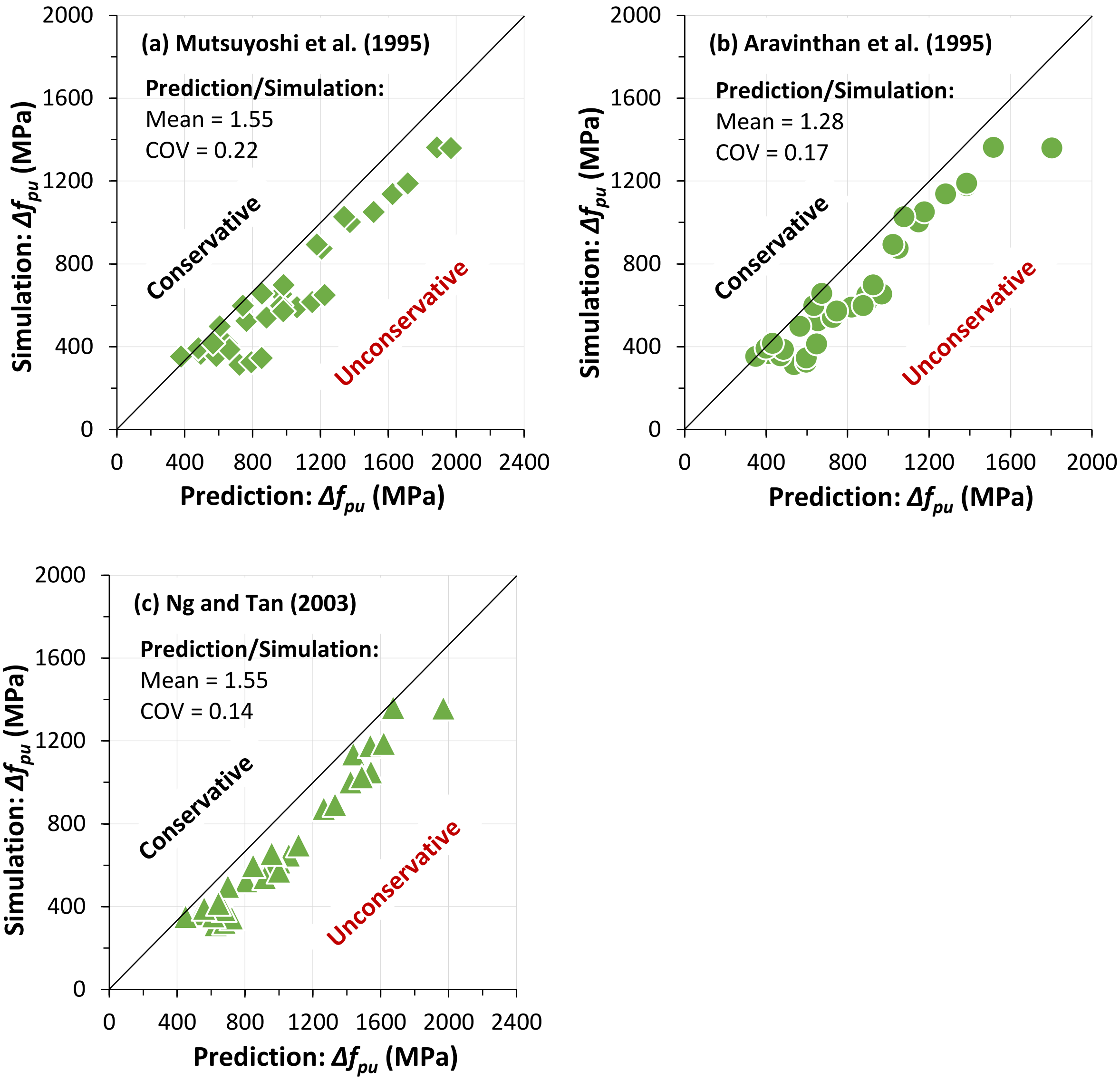

Fig. 18. Ultimate stress increase of external tendons: predictions vs simulation